Martes Cuantico

http://martescuantico.weebly.com

El premio Nobel de Química de 2014
ó
viendo lo que no se puede ver:
microscopios ópticos con resolución nanométrica

Luis Martín-Moreno
lmm@unizar.es

Zaragoza, 4/11/2014

icma / Instituto de Ciencia de Materiales de Aragón /
CSIC
Universidad Zaragoza

Optical Instruments.

~1660

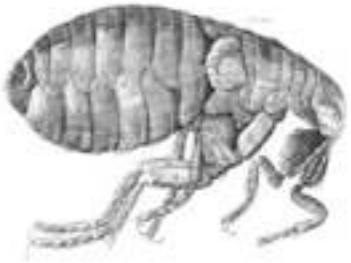

1665. Hooke:
cork cells

1670-80's van Leeuwenhoek:

protozoa, bacterias,

spermatozoids

~1590

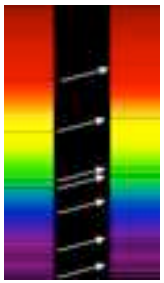

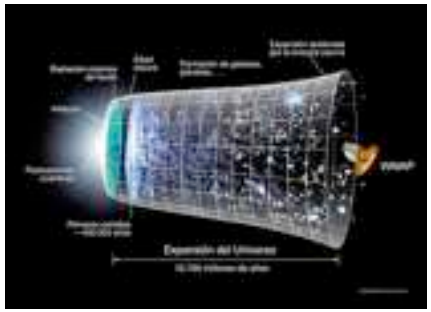

Heliocentrism,
expansion of universe,
extrasolar planets,
dark energy&matter...

1950

The Nobel Prize in Physics 2014 was awarded jointly to

Isamu Akasaki, Hiroshi Amano and Shijo Nakamura

"for the invention of efficient blue light-emitting diodes which has enabled bright and energy-saving white light sources".

The Nobel Prize in Chemistry 2014 was awarded jointly to

William E. Moerner, Stefan W. Hell and Eric Betzig

"for the development of super-resolved fluorescence microscopy".

Special thanks for some viewgraphs

Triple-label imaging with combined techniques.

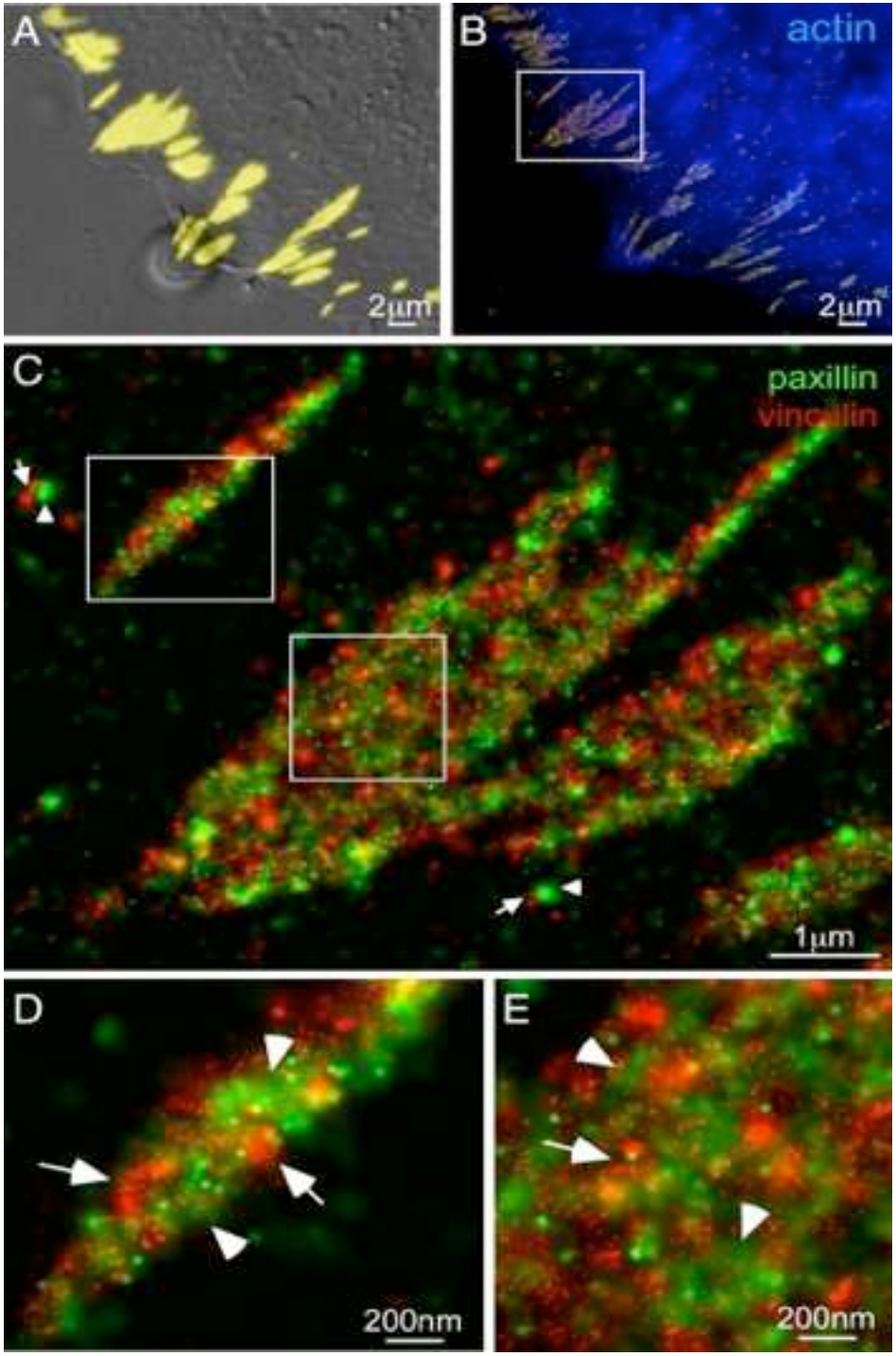

Fig. 5. Triple-label imaging with combined techniques. (*A*) Overlaid DIC and TIRF (yellow) images of paxillin and vinculin coexpressed in an HFF-1 cell. (*B*) Diffraction-limited epi-fluorescence image of mCerulean-tagged actin (blue) overlaid with PALM images of Dronpa-tagged paxillin (green) and tdEos-tagged vinculin (red) shows adhesion complexes at the periphery of the cell aligned with the termini of actin bundles. An expanded view (*C*) of the boxed region in *B* reveals parallel arrays of interwoven paxillin and vinculin aggregates along the length of each AC, as well as possibly nascent adhesion complexes consisting of adjacent paxillin (arrowheads) and vinculin aggregates (arrows). Further magnified views (*D* and *E*) of the boxed regions in *C* indicate other examples of adjacent aggregates of either paxillin (arrowheads) or vinculin (arrows) within larger adhesions.

Shroff H et al. PNAS 2007;104:20308-20313

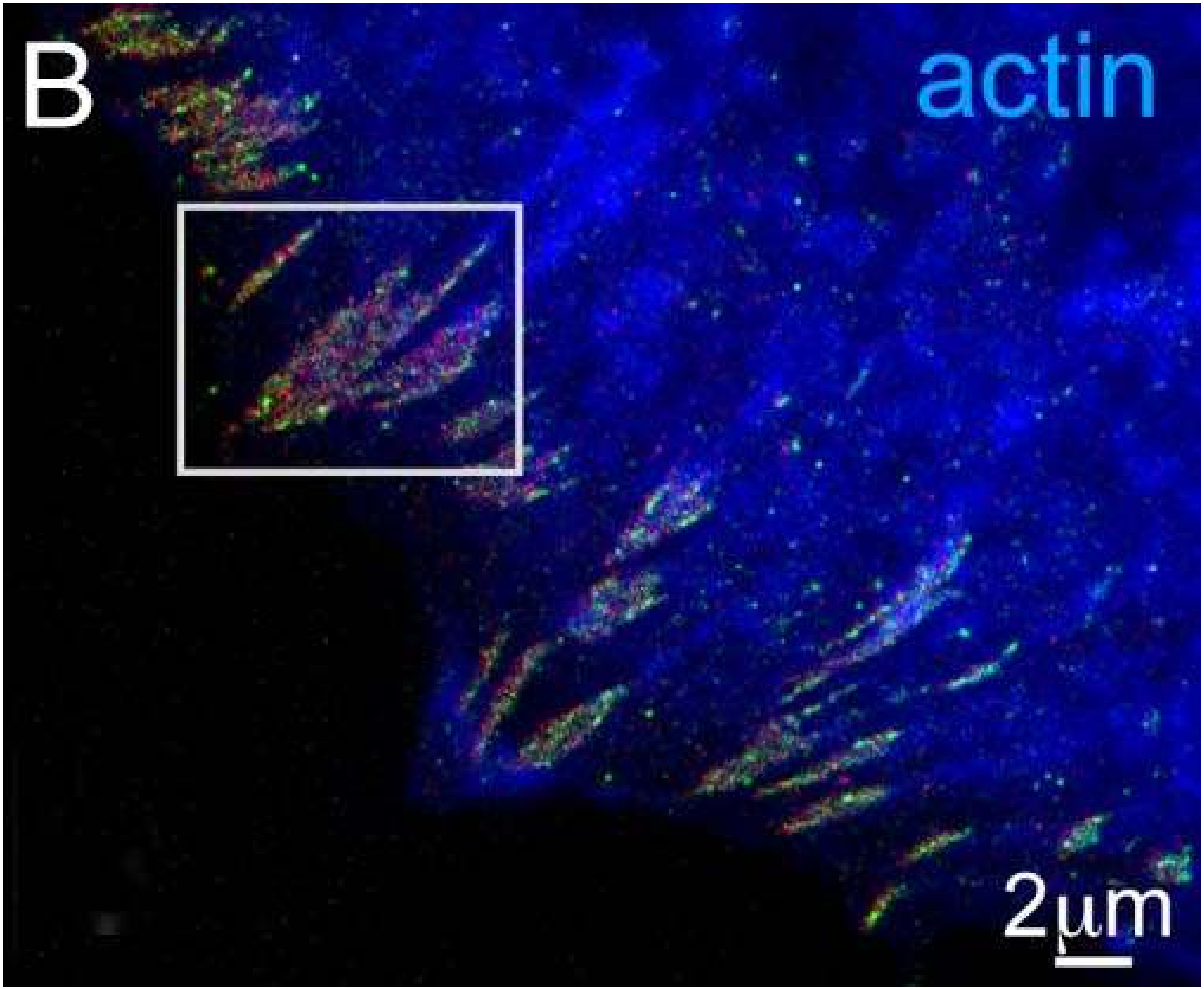
B
actin
2μm

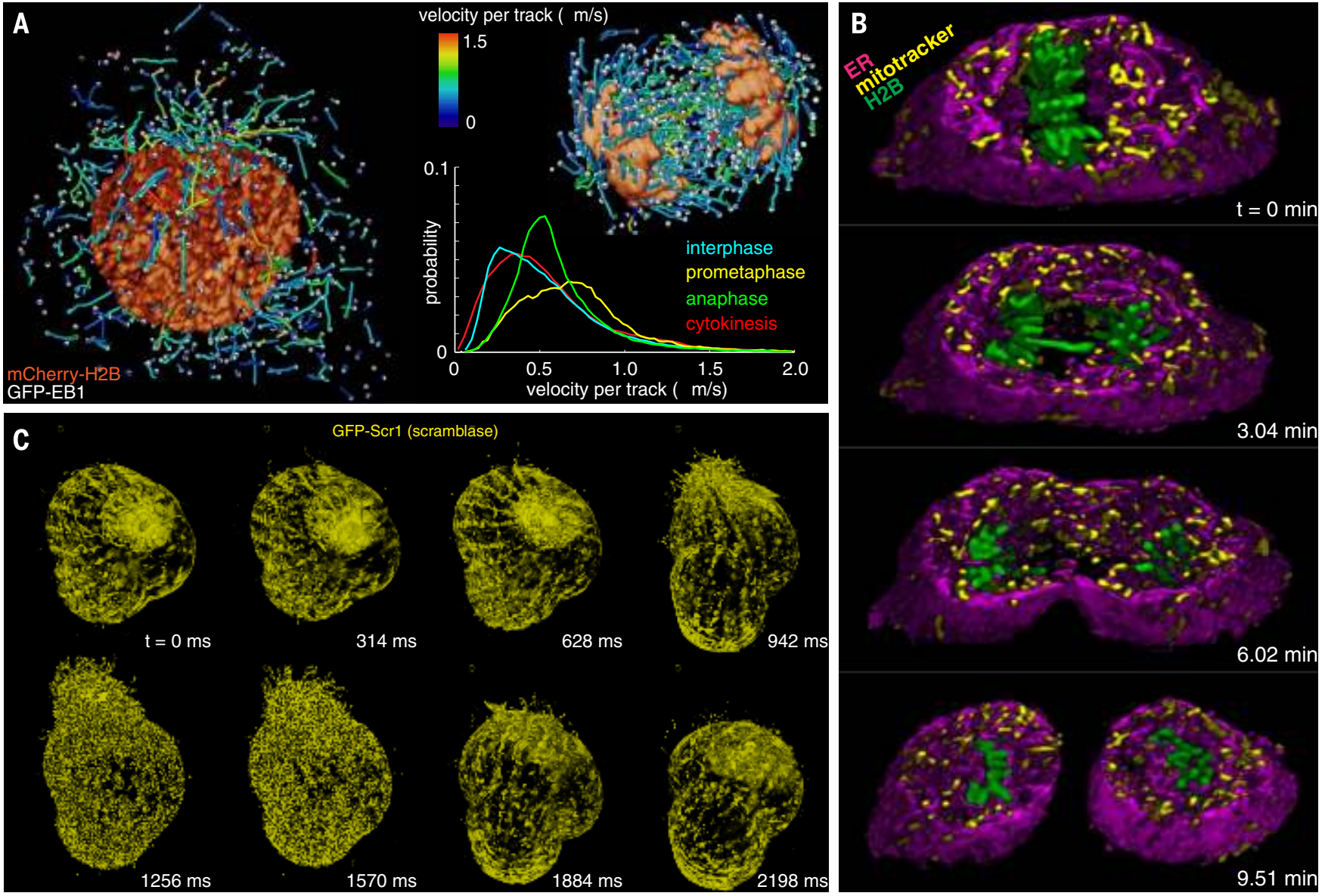

Lattice light-sheet microscopy: Imaging molecules to embryos at high spatiotemporal resolution
Bi-Chang Chen *et al.*
Science **346**, (2014);
DOI: 10.1126/science.1257998

Fig. 4. Intracellular dynamics in three dimensions. (**A**) Cells in prophase (left) and anaphase (right), showing histones and 3D tracks of growing microtubule ends, color-coded by velocity. Color-coding of each track by height (movie S11) or growth-phase lifetime (movie S12) is also possible. Each image in (A) represents a distillation of a few time points from a 4D, two-color data set typically covering hundreds of time points per cell (compare with Movie 5). Graph shows the distribution of growth rates at different stages of mitosis, averaged across 9 to 12 cells (compare with figs. S8 and S9). (**B**) The 3D spatial relationship of histones (green), mitochondria (yellow), and ER (magenta) at four time points during mitosis in a slab extracted from a larger 4D, three-color data set of HeLa cells imaged for 300 time points (compare with Movie 6). (**C**) Volume renderings at eight consecutive time points of a single specimen of the protozoan *T. thermophila* taken from a 4D data set spanning 1250 time points (compare with Movie 7). Imaging at 3 ms per frame in a single plane (compare with movie S13) reveals the motions of individual cilia.

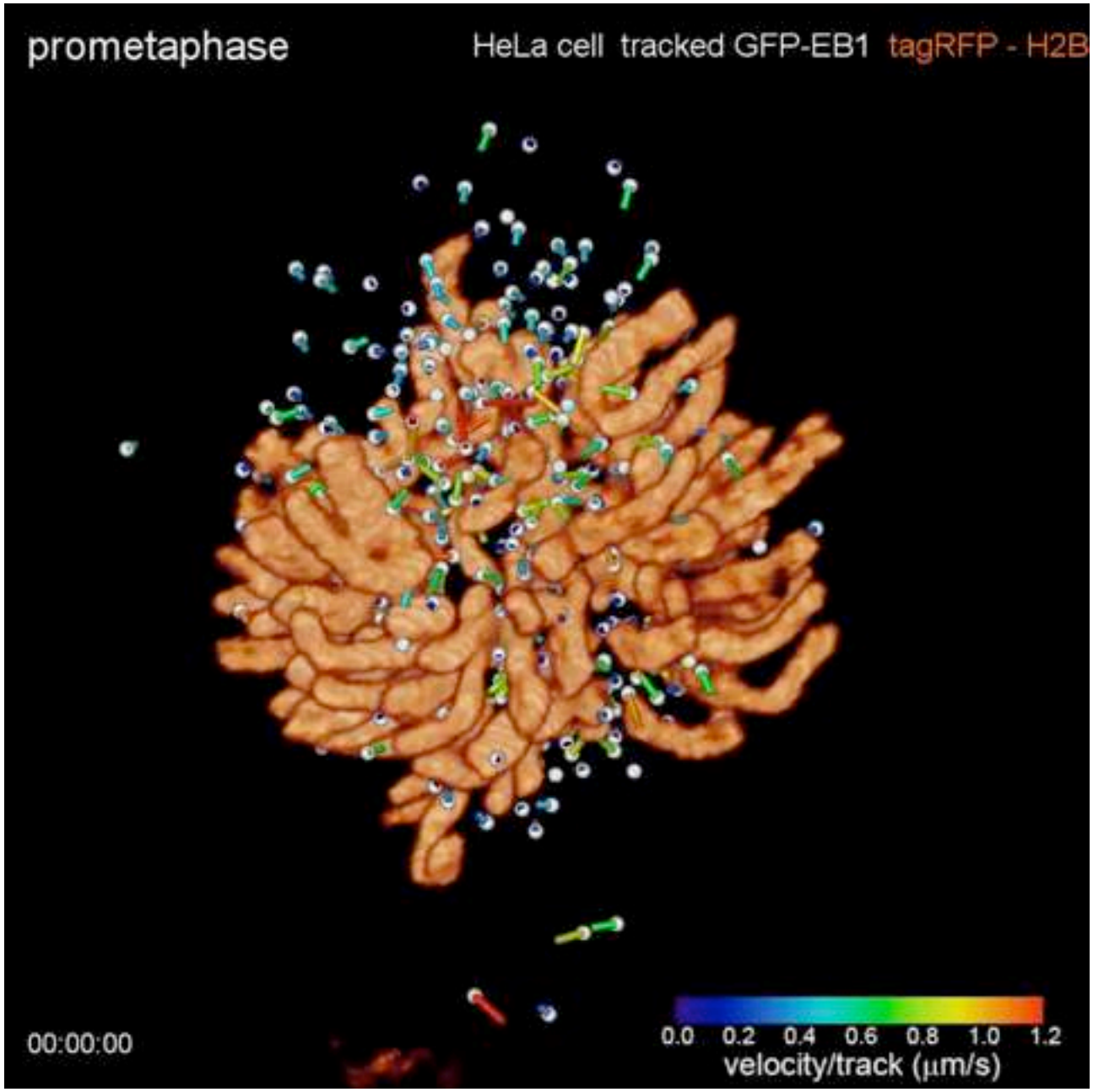
prometaphase
HeLa cell tracked GFP-EB1 tagRFP - H2B
00:00:00
0.0 0.2 0.4 0.6 0.8 1.0 1.2
velocity/track (μm/s)

The diffraction limit.

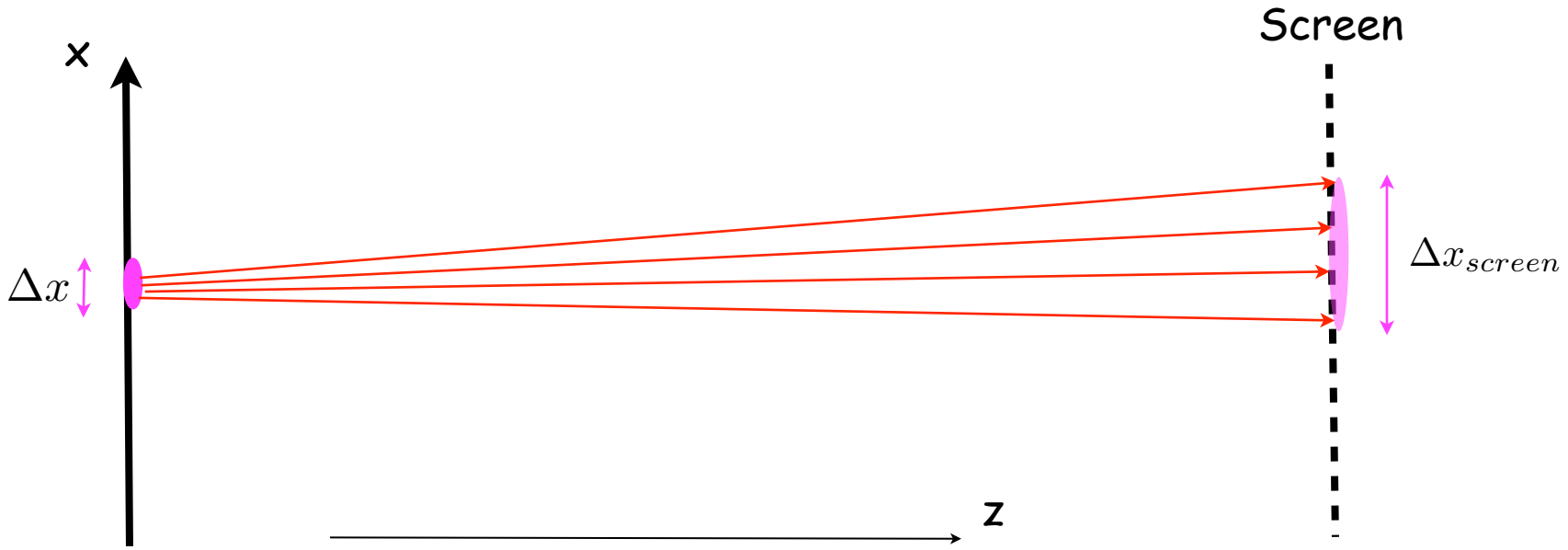

The diffraction limit.

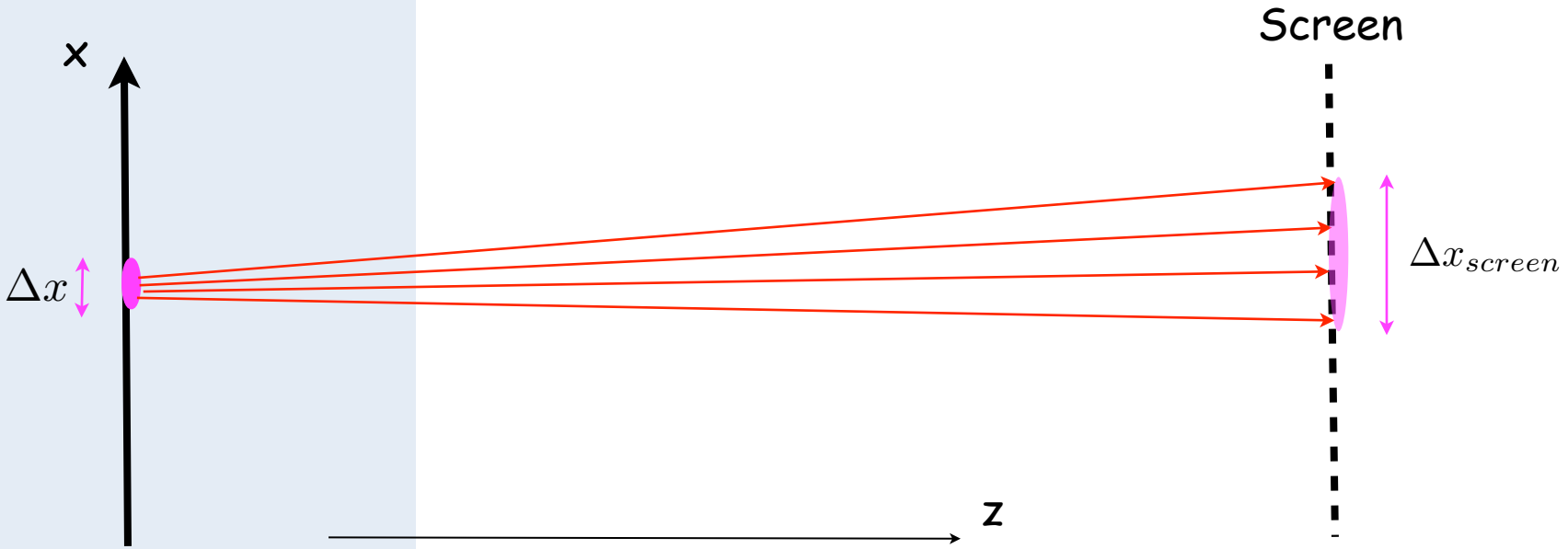

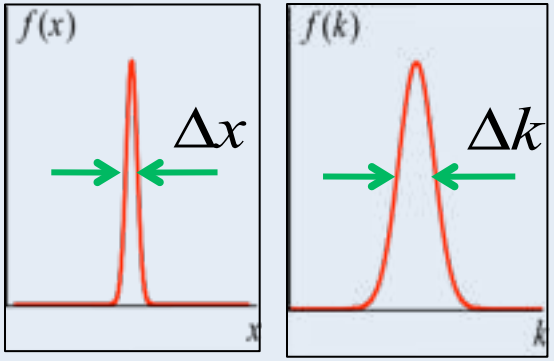

$$f(x) = \int f(k)\ e^{ikx}\ dk$$

$$\Delta k \Delta x \approx 2$$

The diffraction limit.

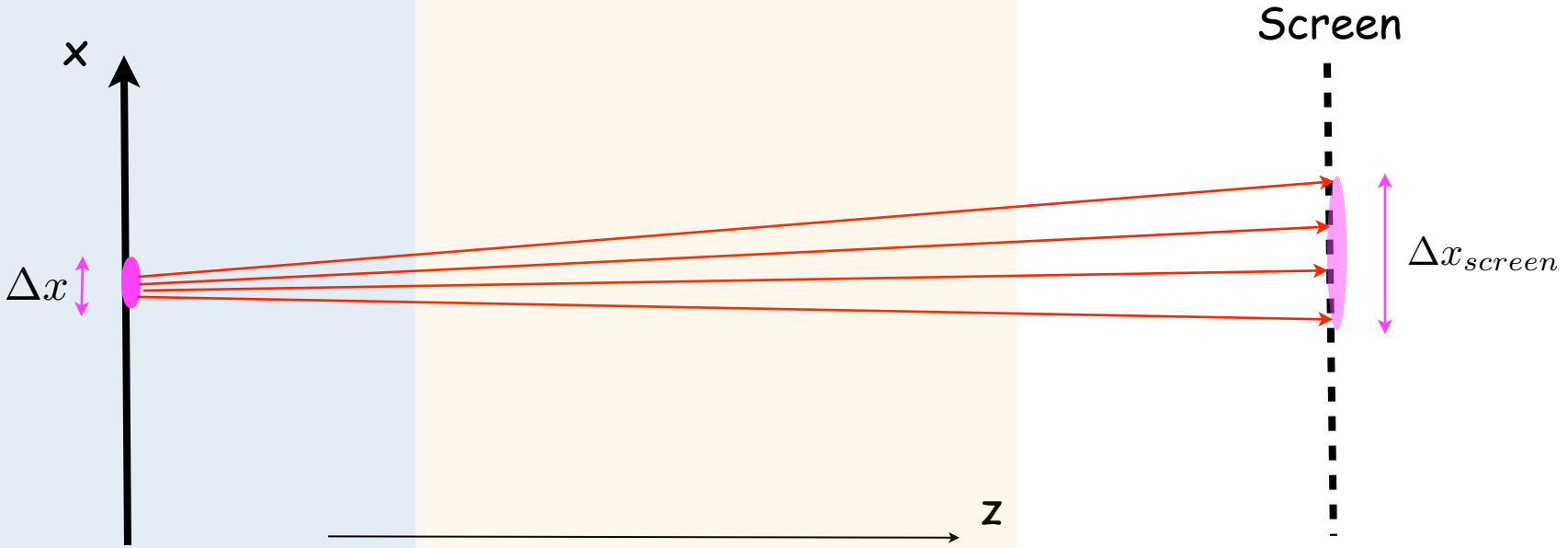

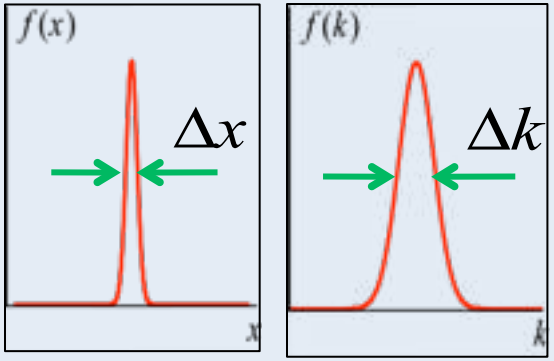

$$\vec{E}(\vec{r}) = \vec{e}_\sigma \, e^{\imath k_x x} \, e^{\imath k_z z}$$

$$|k| = \sqrt{k_x^2 + k_z^2} = \omega / c$$

$$k_z^2 \geq 0 \rightarrow |k_x| < |k|$$

$$f(x) = \int f(k) \; e^{ikx} \; dk$$

$$\Delta k \Delta x \approx 2$$

The diffraction limit.

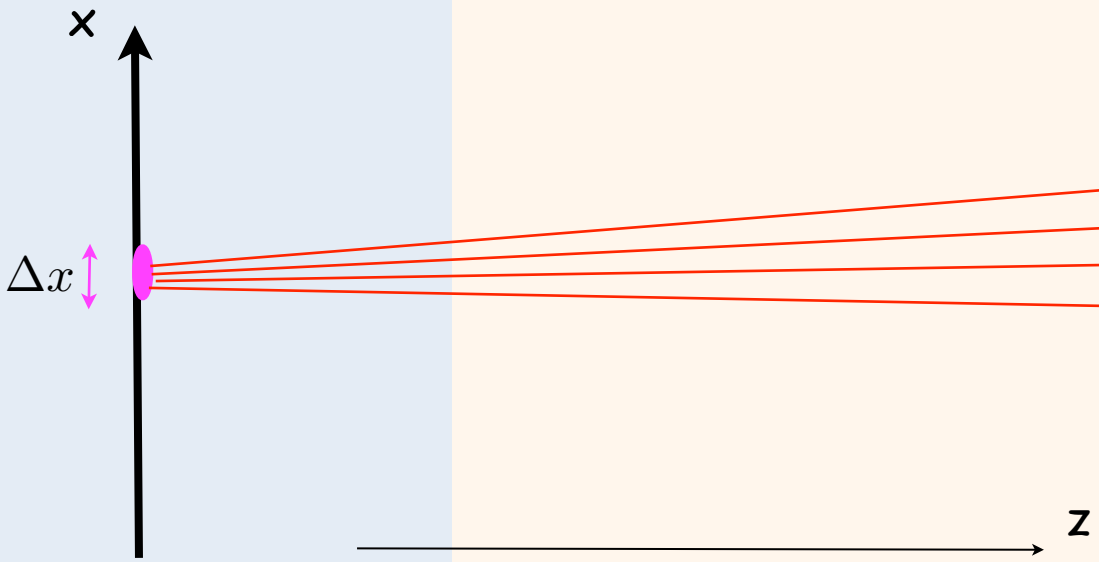

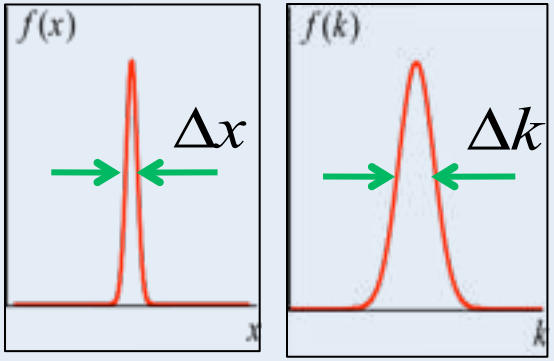

$$\vec{E}(\vec{r}) = \vec{e}_\sigma \, e^{\imath k_x x} \, e^{\imath k_z z}$$

$$|k| = \sqrt{k_x^2 + k_z^2} = \omega / c$$

$$k_z^2 \geq 0 \rightarrow |k_x| < |k|$$

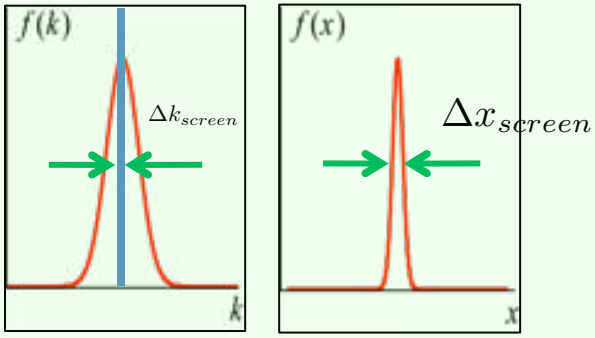

$$f(x) = \int f(k) \; e^{ikx} \; dk$$

$$\Delta k \Delta x \approx 2$$

$$\Delta k_{screen} = 2 \frac{\omega}{c}$$

$$\mathbf{\Delta x_{screen} \approx \lambda / 2}$$

The diffraction limit: influence on spacial resolution

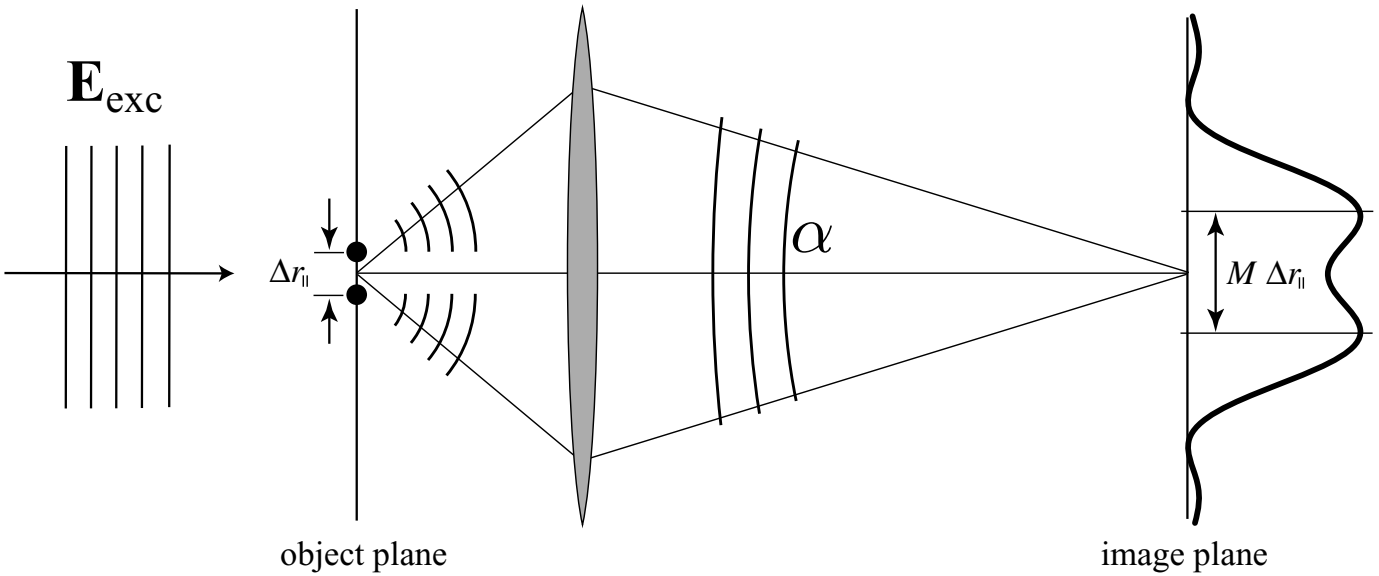

$$Min[\Delta r_n] = \frac{\lambda}{2n\sin\alpha}$$

Principles of Nano-optics, L. Novotny and B. Hecht

The diffraction limit: influence on spacial resolution

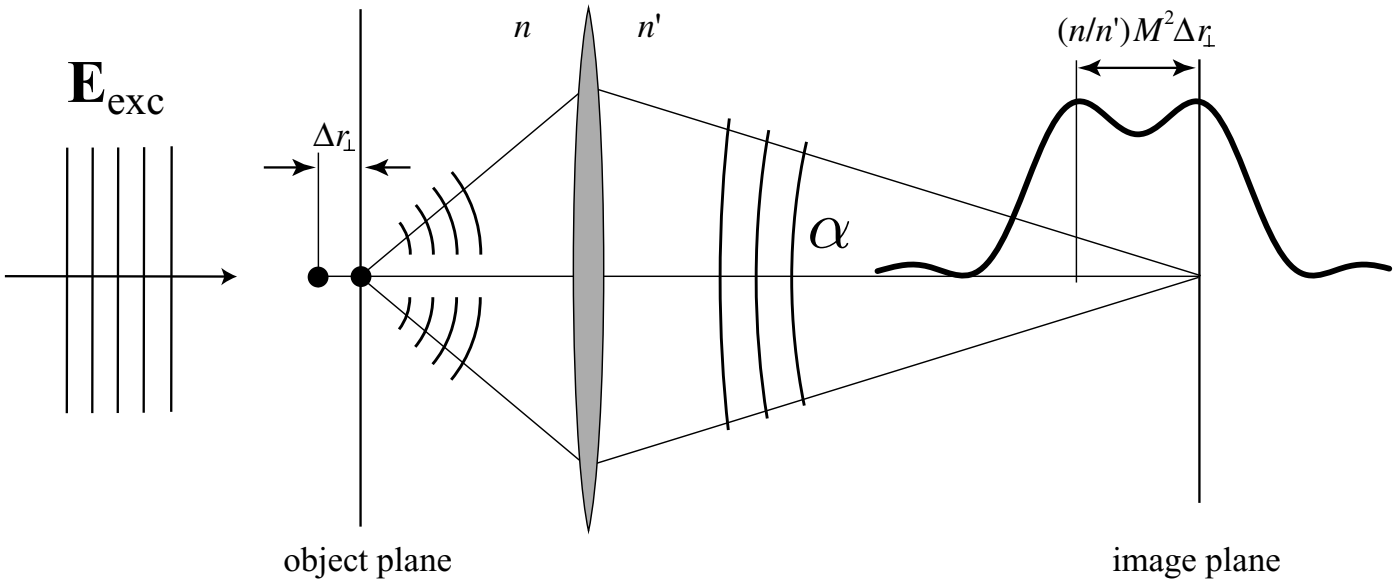

$$Min[\Delta r_\perp] = 2\frac{\lambda}{n\sin^2\alpha}$$

Principles of Nano-optics, L. Novotny and B. Hecht

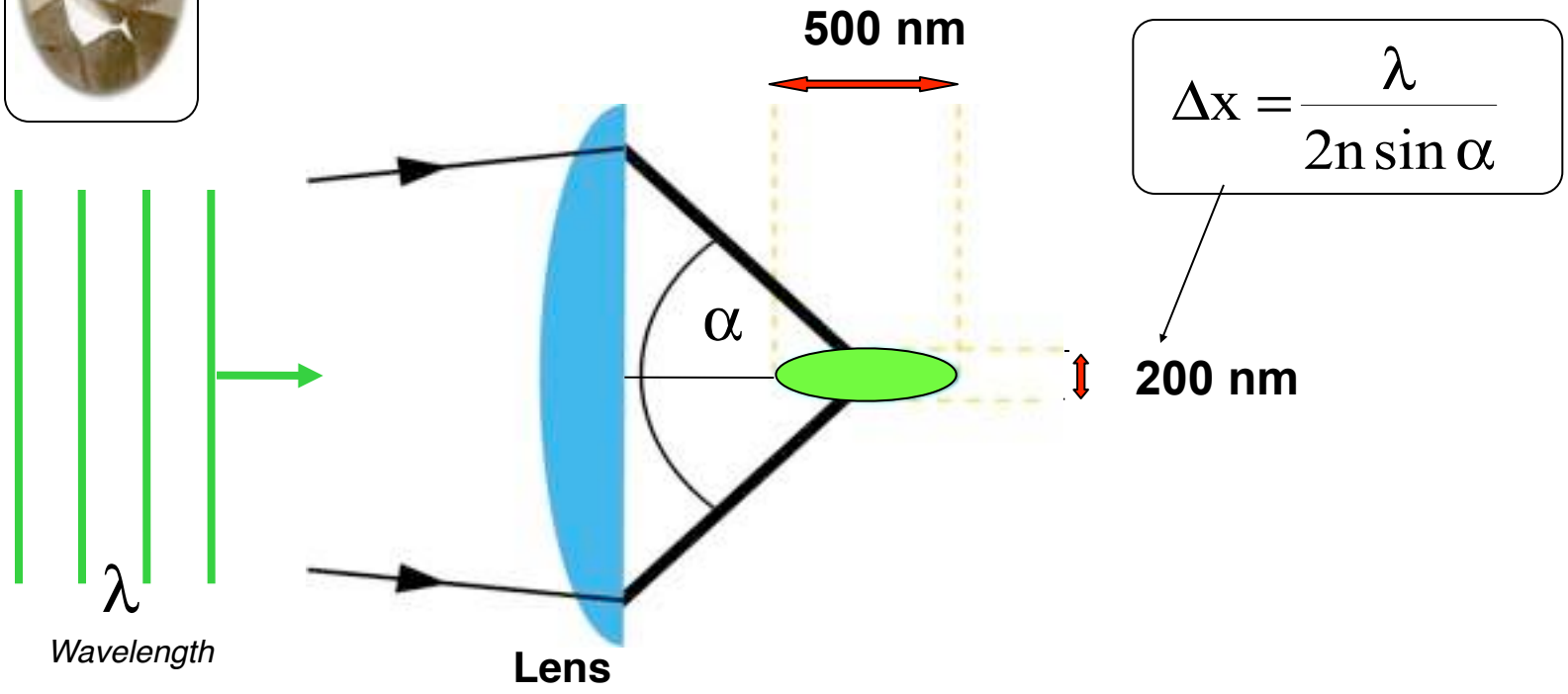

E. Abbe (1873), *Arch. Mikroskop. Anat.* 9, 413.

Axial resolution: confocal microscopy.

Total detected signal does not depend on z -> I

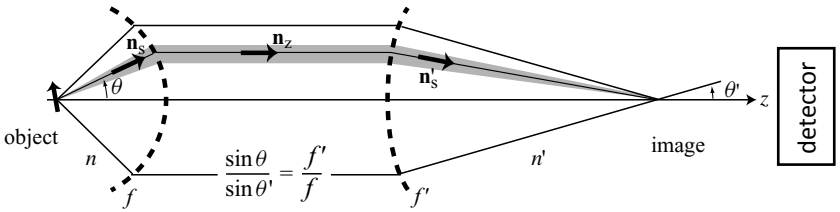

Just placing a pinhole in front of the detector -> I=I(z)

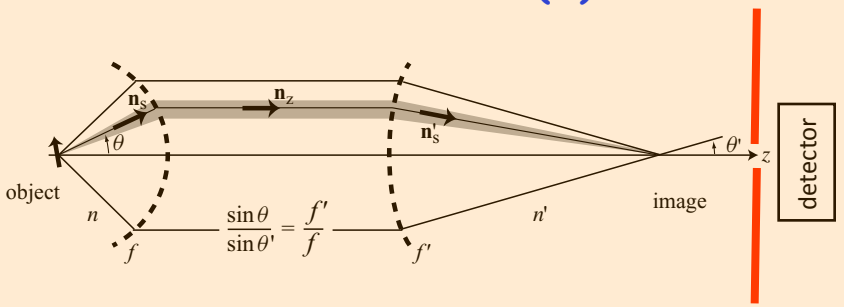

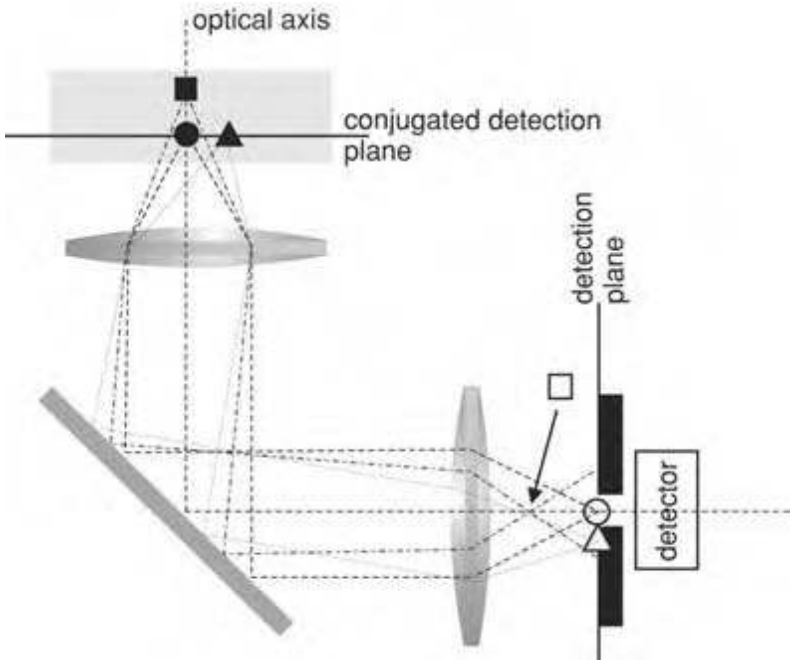

Principles of Nano-optics, L. Novotny and B. Hecht

4Pi- Microscopy: resolution improvement in Z

70 - 140 nm

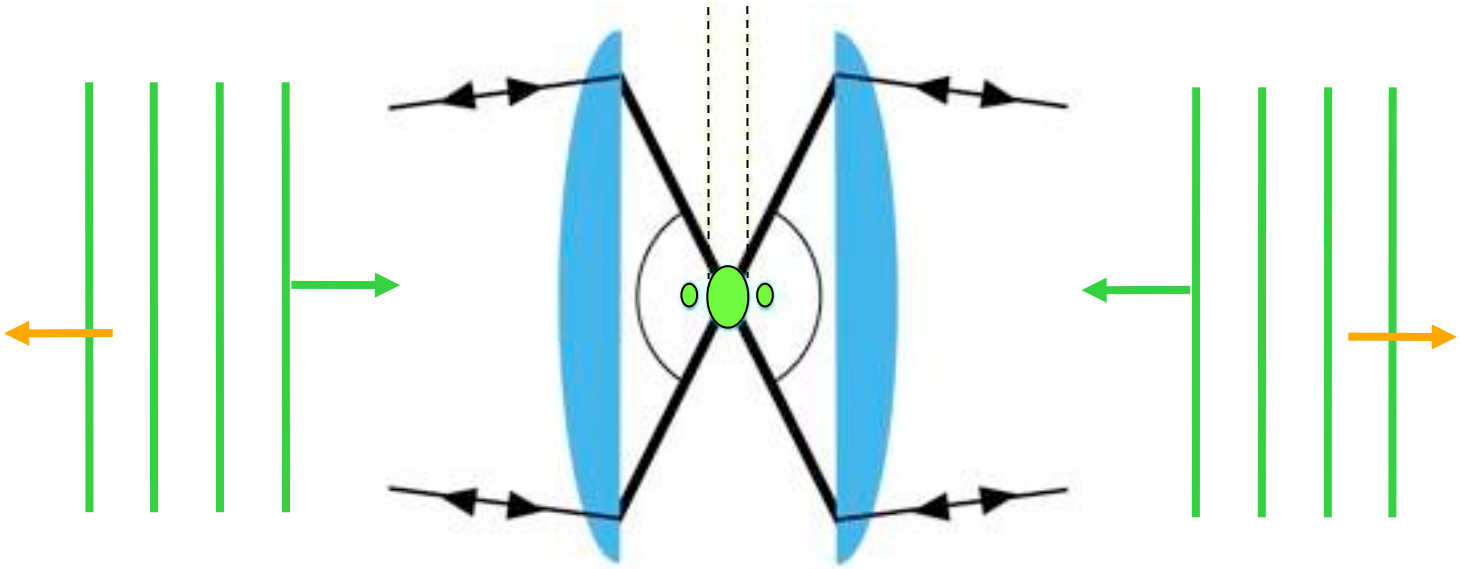

$$\vec{E}^{4Pi}(r,z,\varphi) = \vec{E}_1(r,z,\varphi) + \vec{E}_2(r,-z,\varphi)$$

Coherent illumination and/or fluorescence detection

S.W. Hell (1990), *Europ. Patent* OS 0491289.
S.W. Hell, et al. (1992), *Opt. Commun.* **93**, 277.
M. Schrader, et al. (1998), *Biophys. J.* **75**, 1659.
H. Gugel, et al. (2004), *Biophys. J.* **87**, 4146.

Commercial 4Pi-microscope

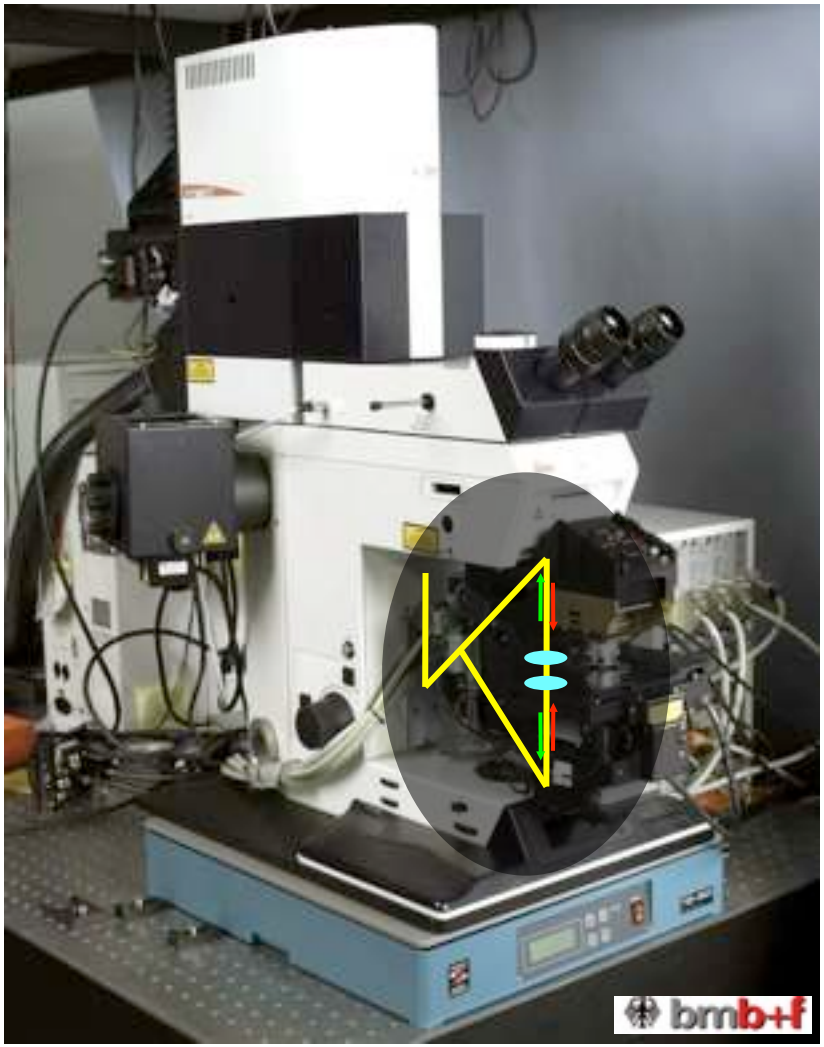

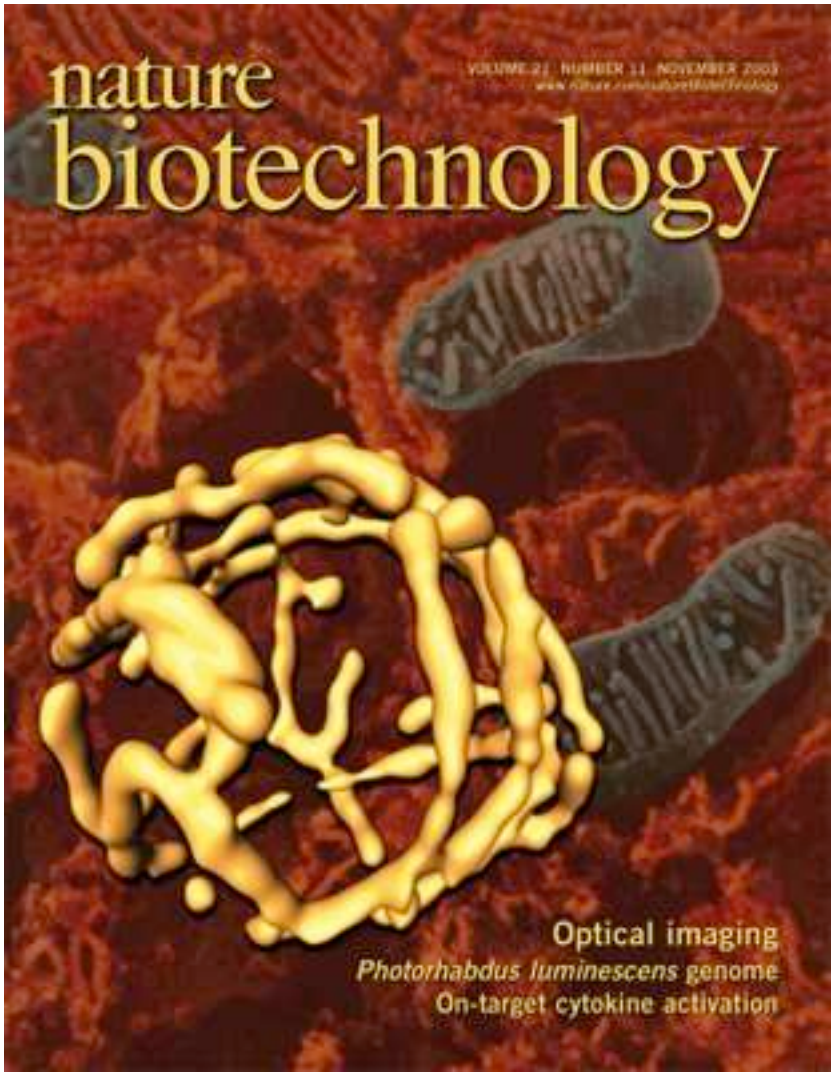

Z- resol < 90 nm (Live cells /aqueous cond.)

H. Gugel, et al. (2004), *Biophys J* **87**, 4146.

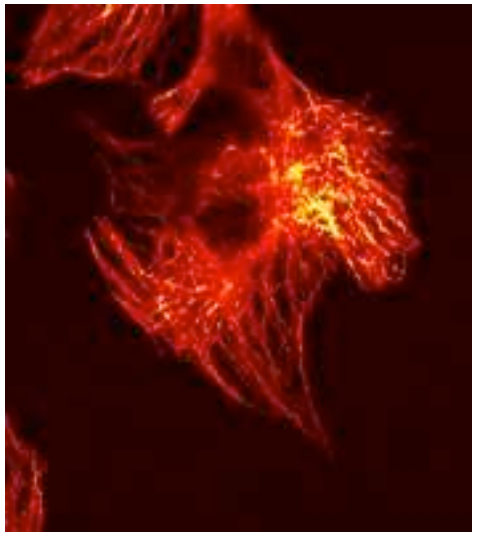

Microtubules, mouse fibroblast
Immunofluor, Oregon Green

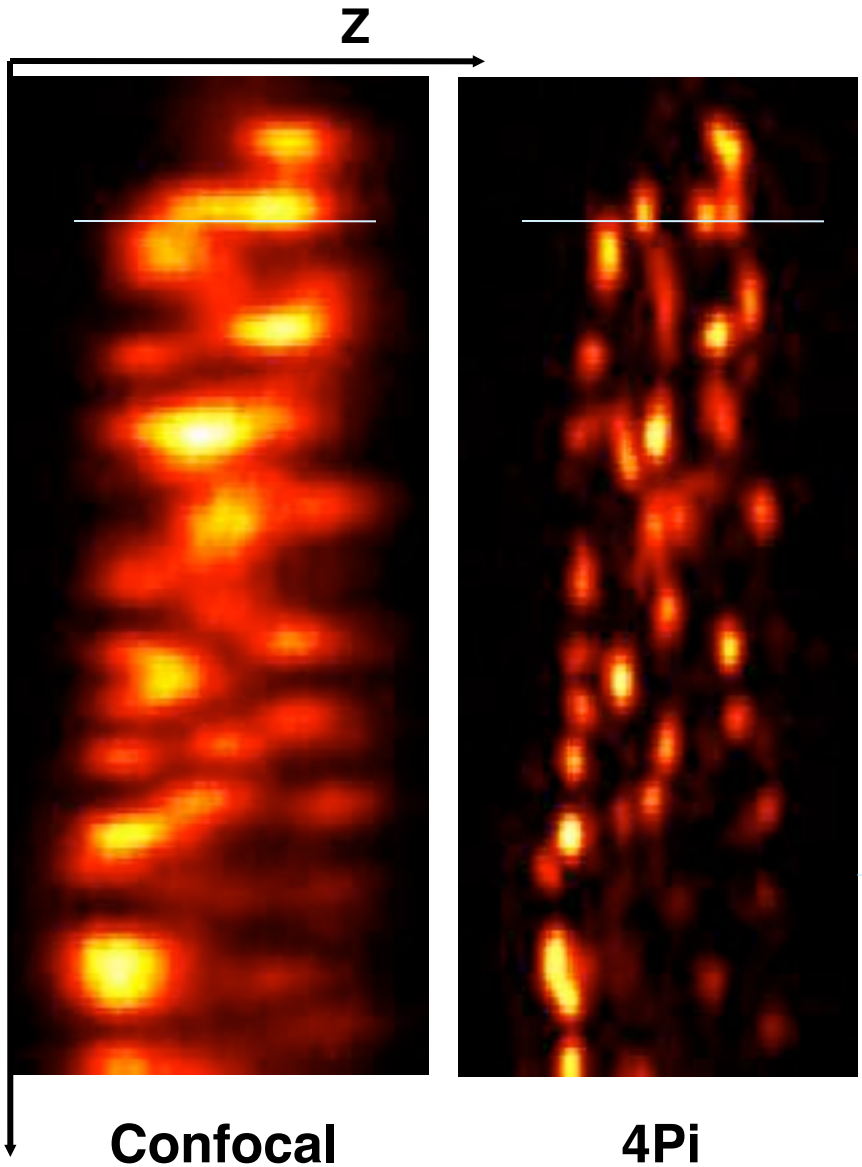

2 µm

2 µm

S.W. Hell, et al. (1992), *Opt. Commun.* **93**, 277.
M. Schrader, et al. (1998), *Biophys. J.* **75**, 1659.
H. Gugel, et al. (2004), *Biophys. J.* **87**, 4146.

Nanophotonics and the diffraction limit.

$$\Delta x \geq \frac{\lambda}{2}$$

Minimum lateral size of light

- For nm resolution we need λ in the nm range -> X rays
- X rays are intensively used for this reason, but have problems (too much energy, so they damage matter)

With light λ is 500-900nm, so $\Delta x \approx 250\text{nm}$

Poor resolution

It is not possible to address single molecules separately

Revisiting the diffraction limit (I)

Beating the diffraction limit: retrieving Fourier components

$$\omega^2 = c^2 k^2 = c^2 (k_x^2 + k_z^2)$$

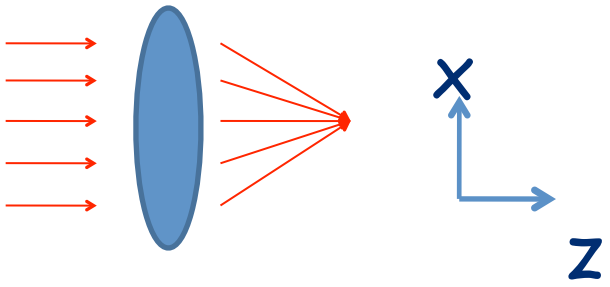

However, if we could play with $k_z^2<0$...

$$k_x^2 = k_\omega^2 - k_z^2 = k_\omega^2 + \left|k_z^2\right|$$ as large as we want

$$\rightarrow \quad \Delta x$$ arbitrarily small

$$k_z^2 < 0 \longrightarrow k_z = \pm i \left|k_z\right| \quad \rightarrow \quad E(\vec{r}) = \vec{e}_\sigma \; e^{ik_x x} e^{ik_z z}$$

Beating the diffraction limit: retrieving Fourier components

$$\vec{E}(\vec{r}) = \overrightarrow{e_\sigma}\ e^{ik_x x}\ e^{\pm|k_z|z}$$

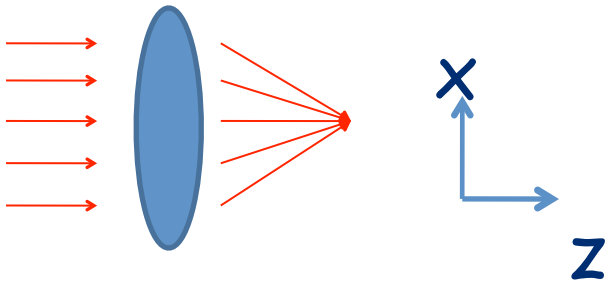

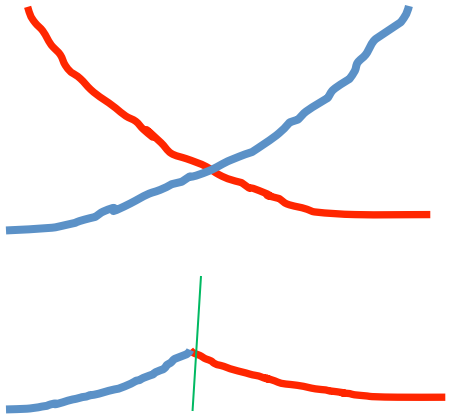

These waves can not exist
in uniform media, but...

exist if there are interfaces

Problem:

the field is only intense close to the interfase

-> near-field optics

Scanning probe techniques

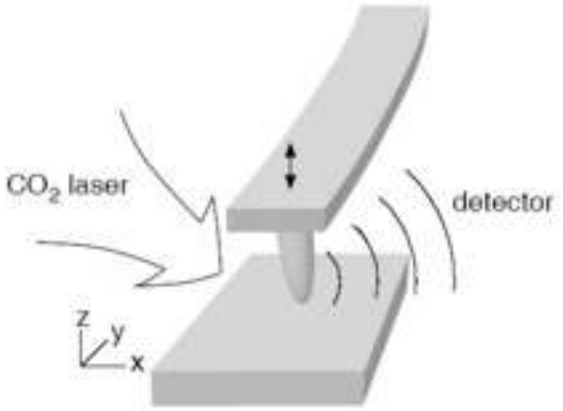

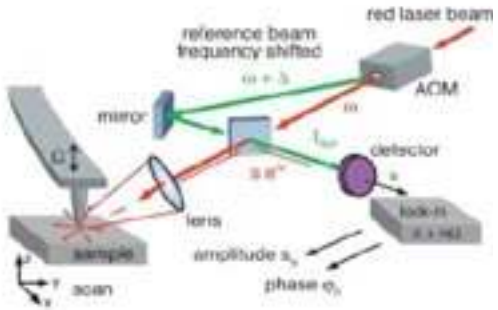

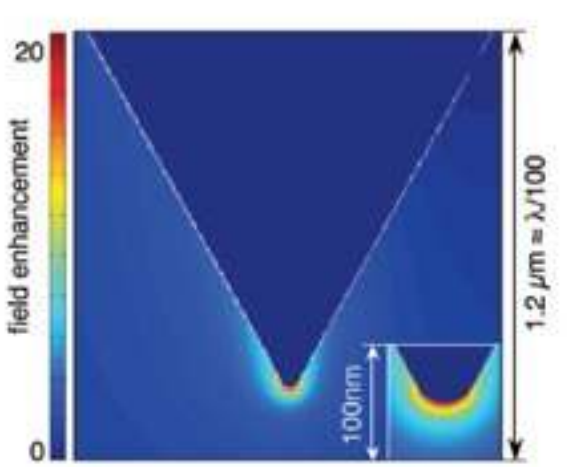

1. Images of SiC islands (metallic at 10 μm)

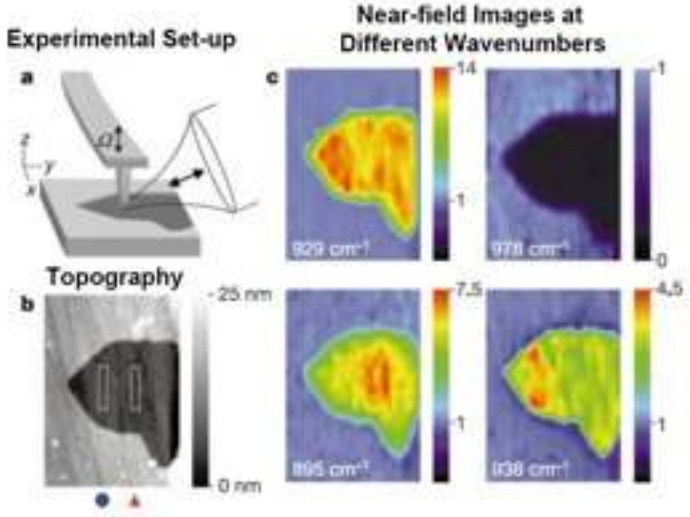

Hillenbrand et al, Nature vol. 418, pp. 159-162 (2002)

2. Fields in metallic environments

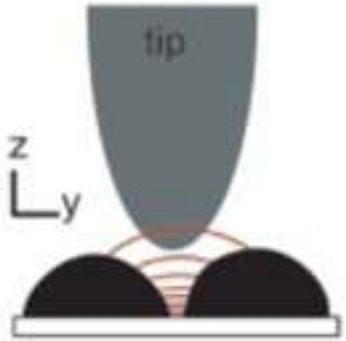

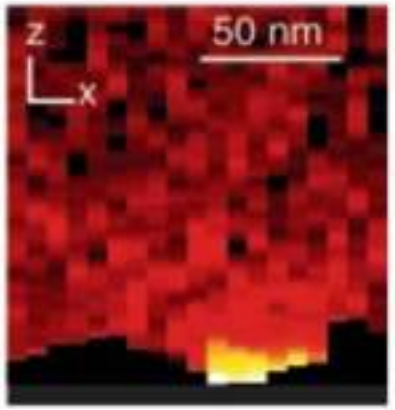

Revisiting the diffraction limit (II)

But,
Abbe's limit is related to two simultaneously emitting emitters.

If one could scan them independently...

Beating the diffraction limit: measuring 1 emitter at the time

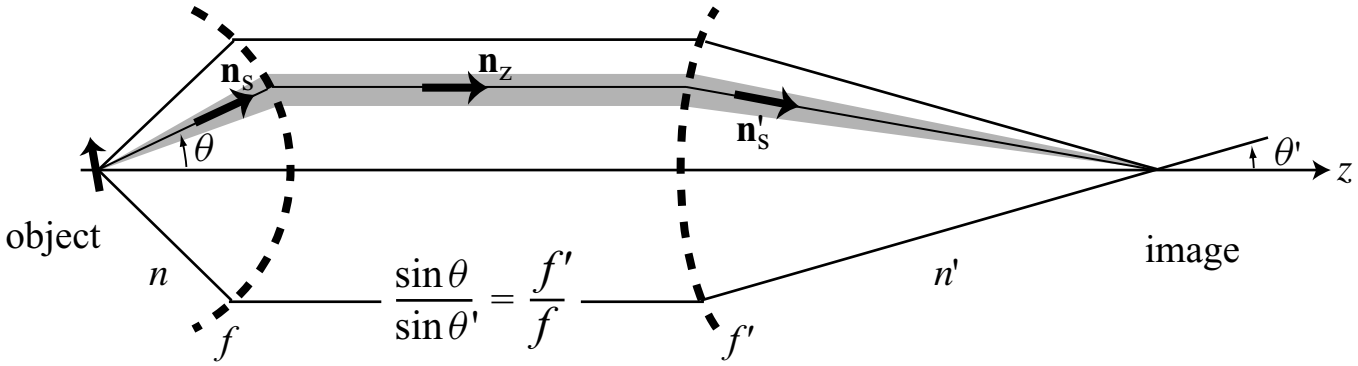

Point spread function

$$\lim_{\theta_{\max} \ll \pi/2} \left|\mathbf{E}(x, y, z=0)\right|^2 = \frac{\pi^4}{\varepsilon_0^2 n n'} \frac{\mu_x^2}{\lambda^6} \frac{\mathrm{NA}^4}{M^2} \left[2 \frac{J_1(2\pi\tilde{\rho})}{(2\pi\tilde{\rho})}\right]^2, \qquad \tilde{\rho} = \frac{\mathrm{NA}\rho}{M\lambda}.$$

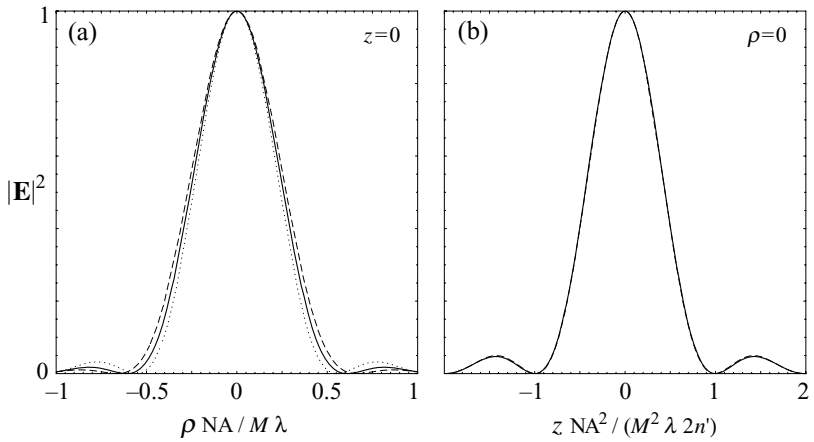

Spatial resolution is NOT position accuracy!

$$\Delta x = \frac{\lambda}{2n \sin\alpha \sqrt{N}}$$

Principles of Nano-optics, L. Novotny and B. Hecht

Fluorophores

Fluorescence is the emission of light by a substance that has absorbed light or other electromagnetic radiation.

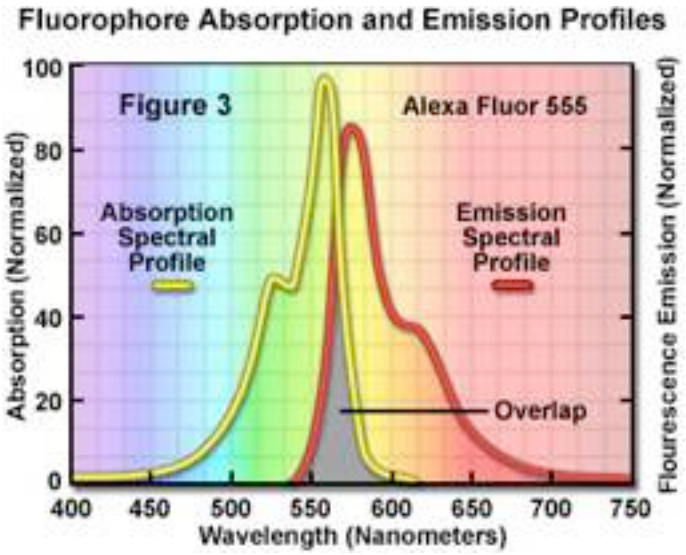

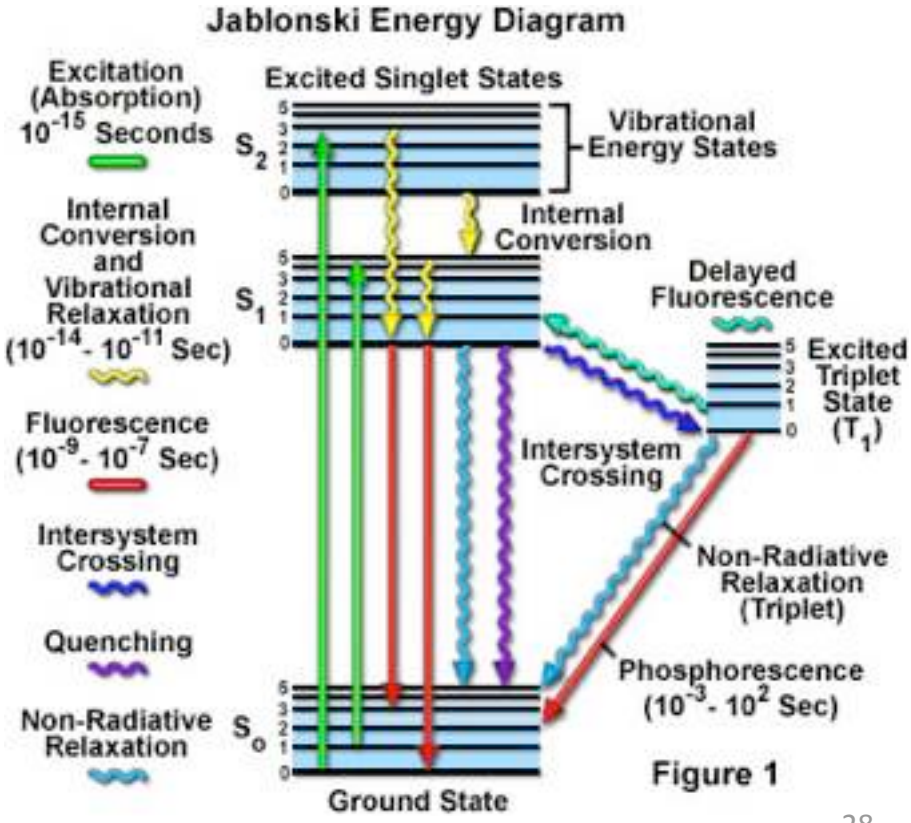

Fluorescence excitation in dilute samples

VOLUME 62, NUMBER 21 PHYSICAL REVIEW LETTERS 22 MAY 1989

Optical Detection and Spectroscopy of Single Molecules in a Solid

W. E. Moerner and L. Kador[a]

VOLUME 65, NUMBER 21 PHYSICAL REVIEW LETTERS 19 NOVEMBER 1990

Single Pentacene Molecules Detected by Fluorescence Excitation in a *p*-Terphenyl Crystal

M. Orrit and J. Bernard

Inhomogeneous broadening:
linewidth associated to emission of
MANY fluorophores
in different local environments

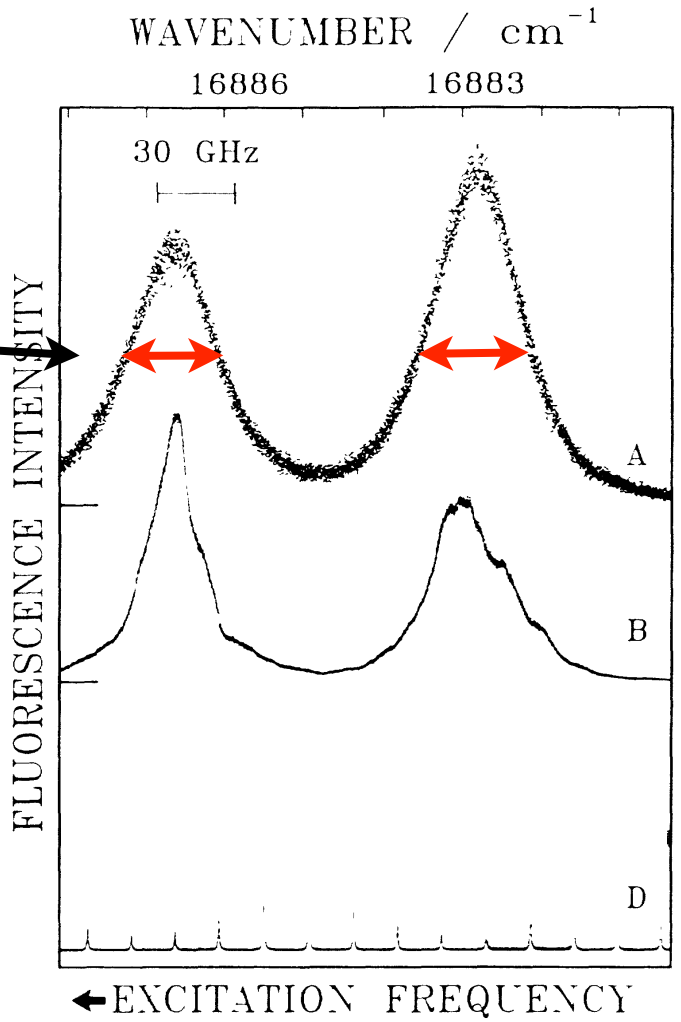

FIG. 1. O_1,O_2 region of the fluorescence excitation spectra of pentacene in different *p*-terphenyl crystals. Curve *A*, thick melt-grown crystal showing the Gaussian inhomogeneous bands. *B*, sublimation flake presenting narrower bands and substructure presumably due to cooling-induced defects. *C*, spectrum of a very small volume of a sublimation flake. The dots are the narrow excitation peaks of individual molecules. *D*, calibration spectrum of an etalon.

Fluorescence excitation in dilute samples

VOLUME 65, NUMBER 21 PHYSICAL REVIEW LETTERS 19 NOVEMBER 1990

Single Pentacene Molecules Detected by Fluorescence Excitation in a *p*-Terphenyl Crystal

M. Orrit and J. Bernard

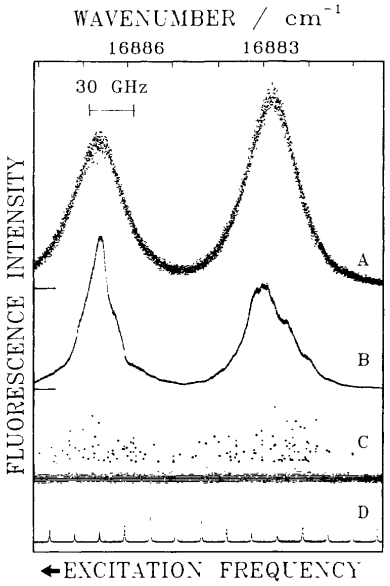

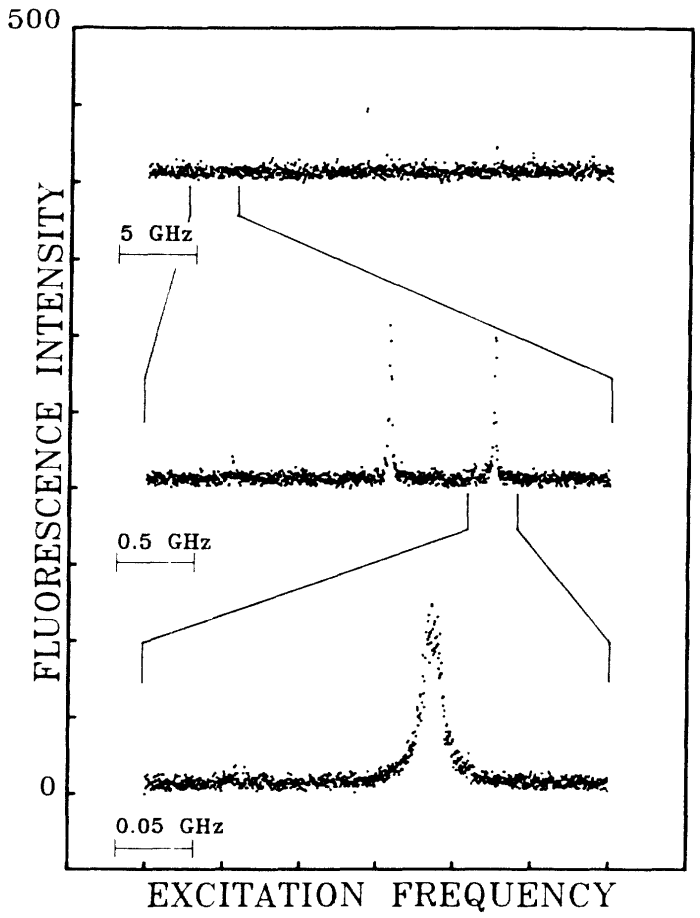

FIG. 2. Shape of a single molecule's excitation peak at different frequency scales. The bottom spectrum is approximately Lorentzian with FWHM about 12 MHz. The vertical scale is in counts/channel.

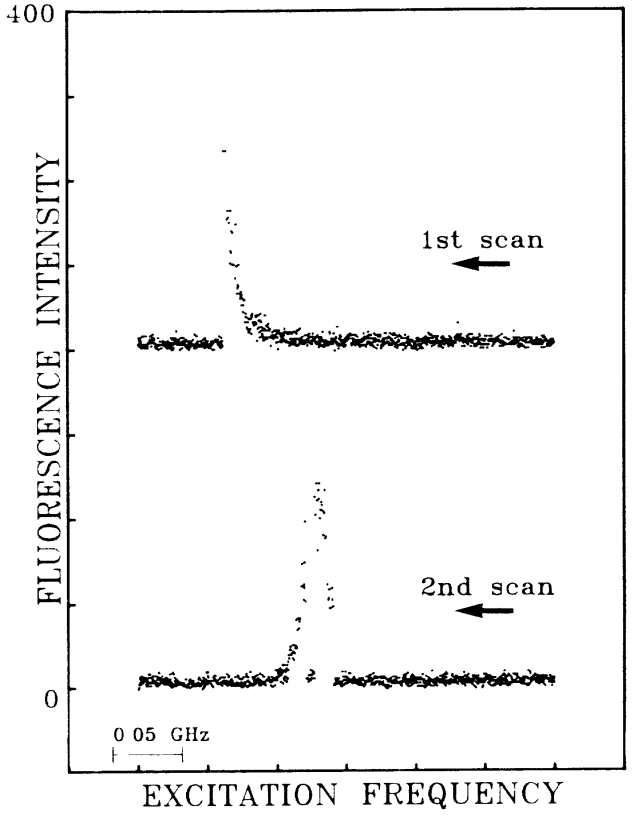

FIG. 4. Two successive scans of the excitation spectrum of a single molecule suggesting a photophysical hole-burning process. The sudden intensity falls and surges might arise from the flip-flops of a two-level system in the neighborhood of the molecule. The time per channel was 0.08 s and a scan lasted about 1 min. The vertical scale is in counts/channel.

Visualizing dynamics of molecular motors

Myosin V Walks Hand-Over-Hand: Single Fluorophore Imaging with 1.5-nm Localization

Ahmet Yildiz *et al.*

Science **300**, 2061 (2003);
DOI: 10.1126/science.1084398

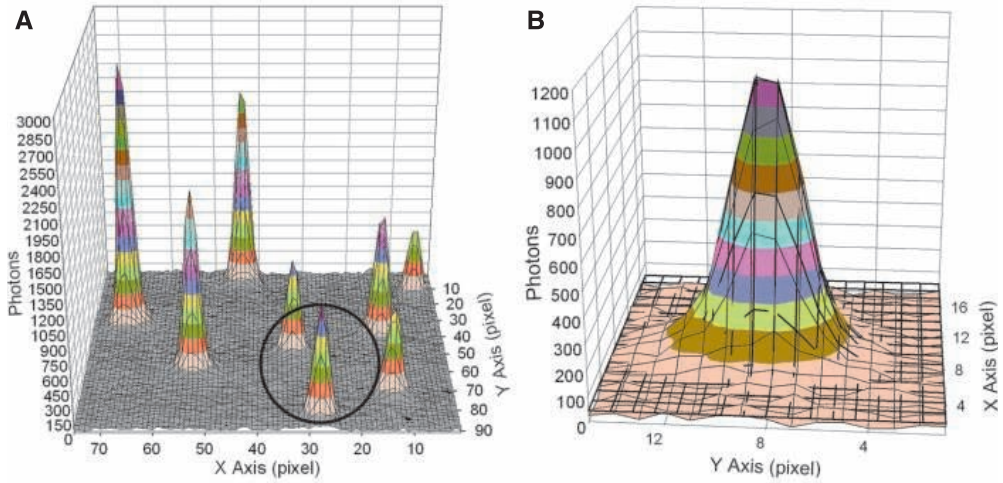

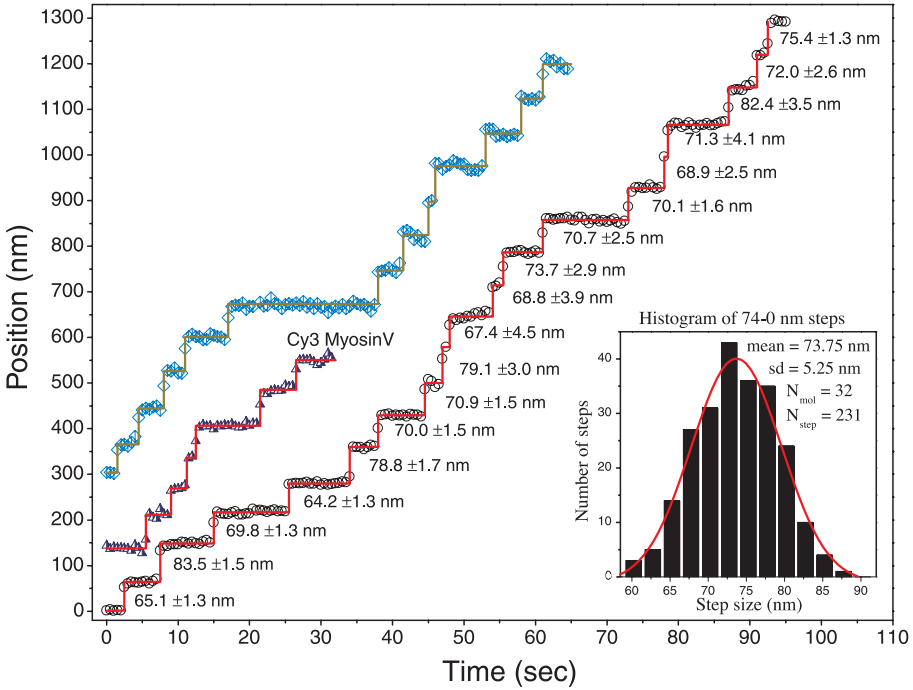

Fig. 3. Stepping traces of three different myosin V molecules displaying 74-nm steps and histogram (inset) of a total of 32 myosin V's taking 231 steps. Calculation of the standard deviation of step sizes can be found (*14*). Traces are for BR-labeled myosin V unless noted as Cy3 Myosin V. Lower right trace, see Movie S1.

What about dense fluorophore concentrations?

Can we excite nearby fluorophores sequentially?

Fluorescence inhibition from stimulated emission

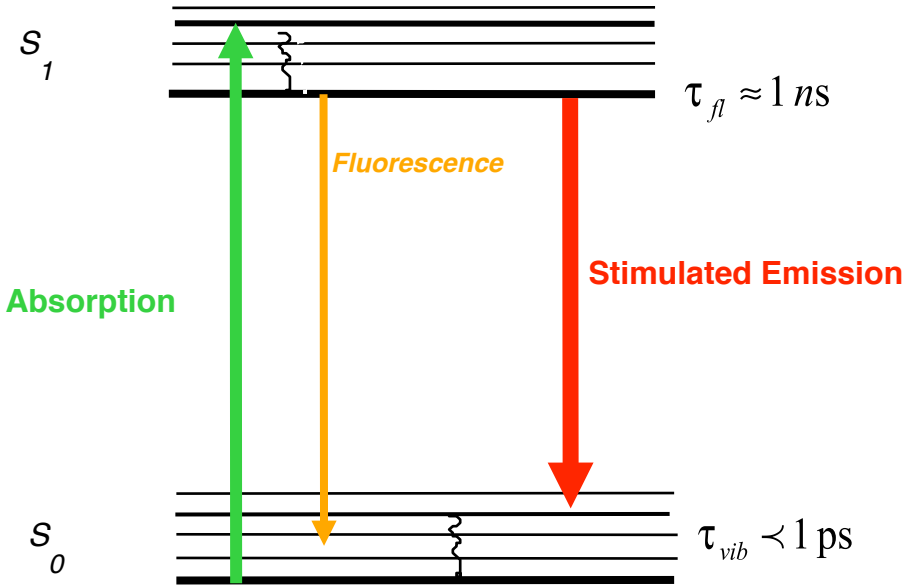

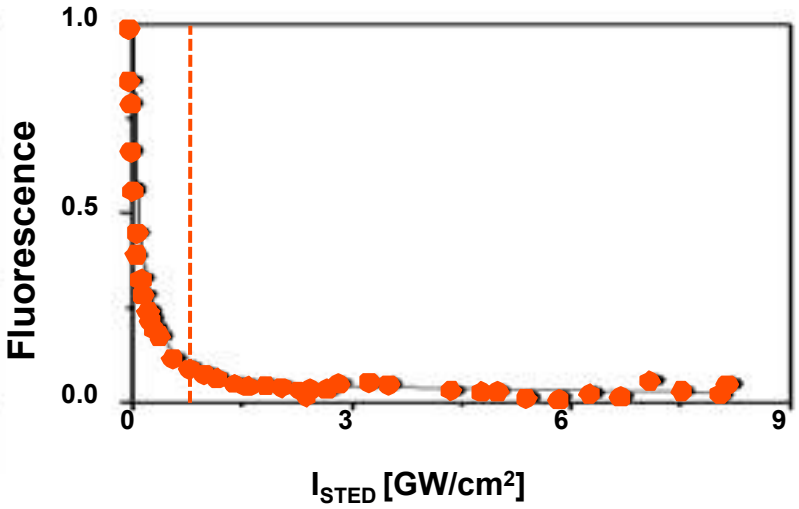

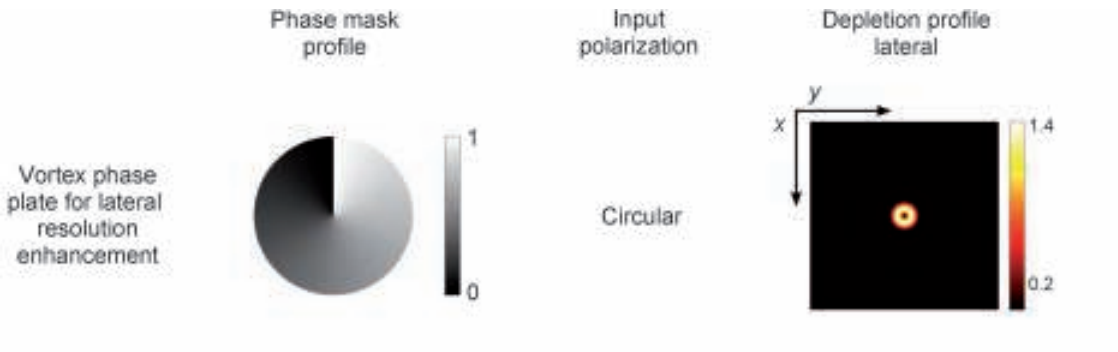

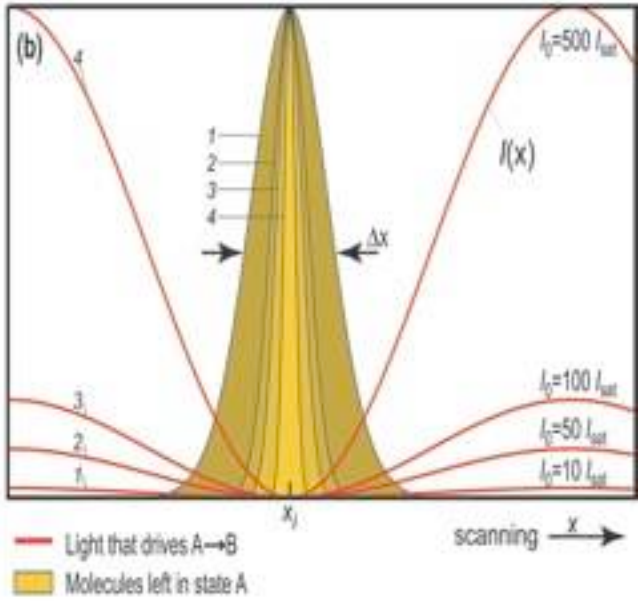

STED Microscopy

S.W. Hell & J. Wichmann (1994), *Opt. Lett.* **19**, 780.

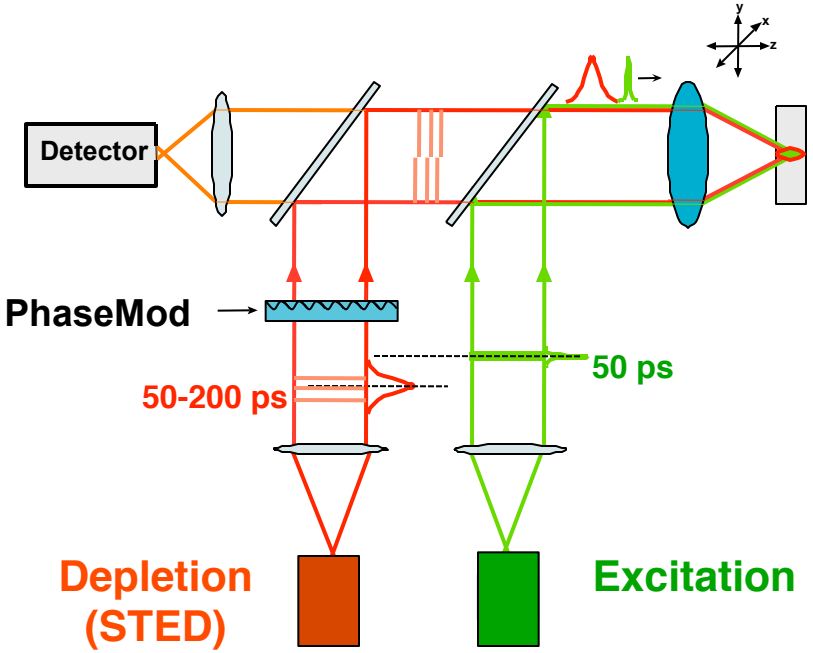

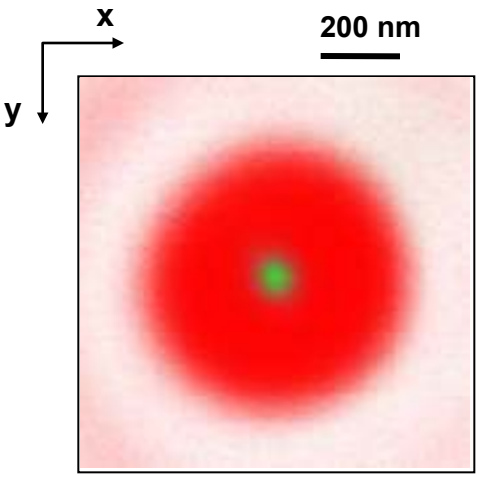

The stronger the STED beam the narrower the fluorescent spot!

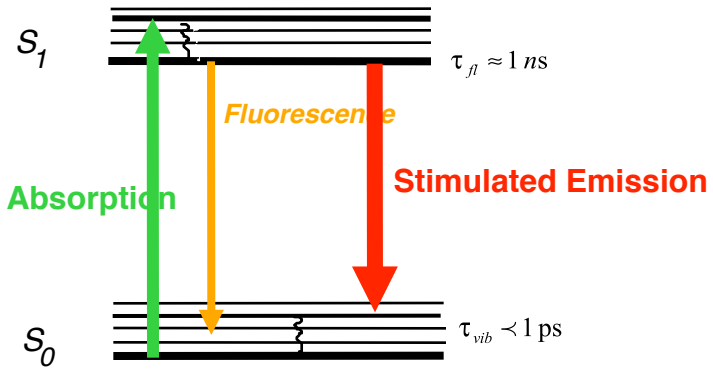

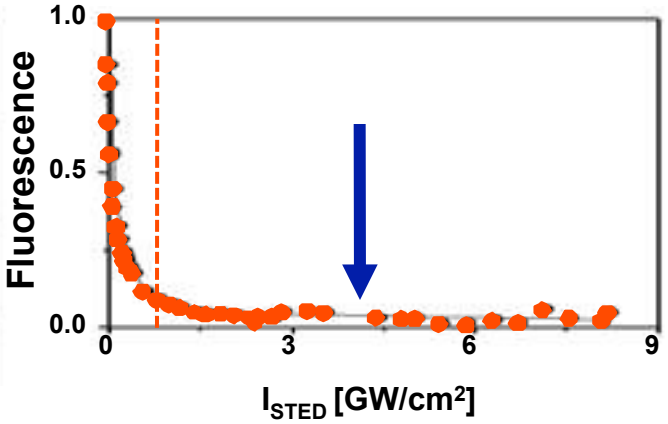

Heavy subunit of neurofilaments in neuroblastoma

Confocal

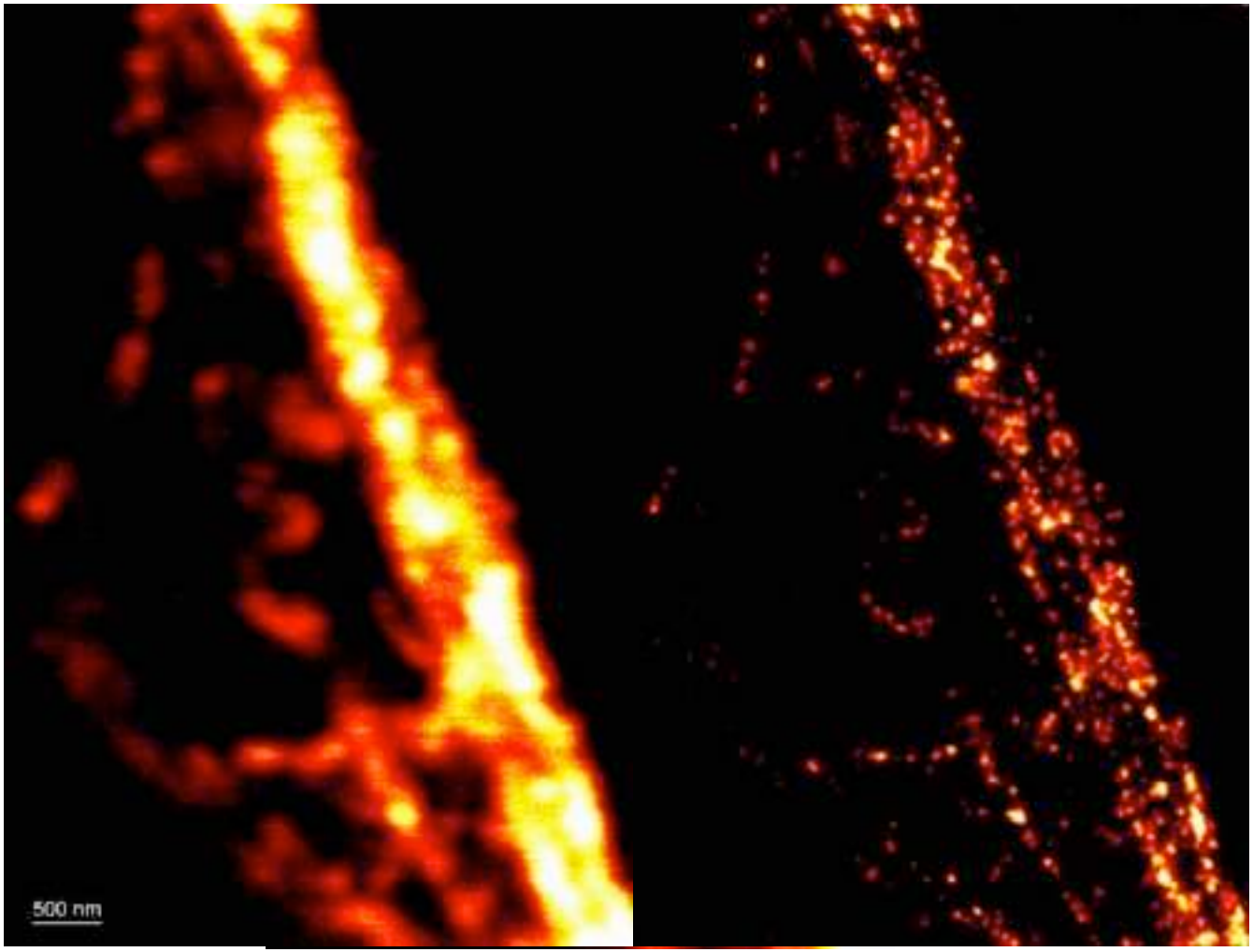

STED

G. Donnert, et al. (2006), *PNAS* **103**, 11440.

STED microscopy

- Resolution is not limited by the wavelength of light!

- Resolution just depends on the level of fluorescence depletion.

- Resolution at the molecular scale is possible with visible light and regular lenses!

- Resolution follows a new law; a modification of Abbe's law:

$$\Delta x \approx \frac{\lambda}{2n \sin\alpha \sqrt{1 + I/I_{sat}}}$$

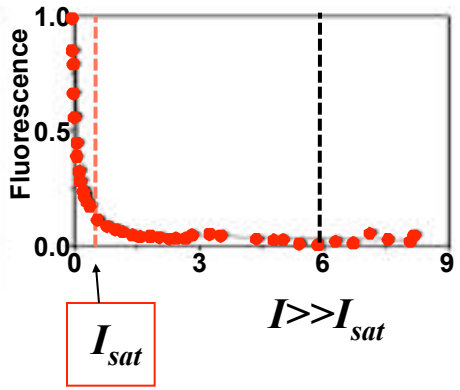

S.W. Hell (2003), *Nature Biotech.* **21**, 1347.
S.W. Hell (2004), *Phys. Lett. A* **326**, 140.
V. Westphal & S.W. Hell (2005), *Phys. Rev. Lett.* **94**, 143903.

Max Planck Society

Sharpest focal spot

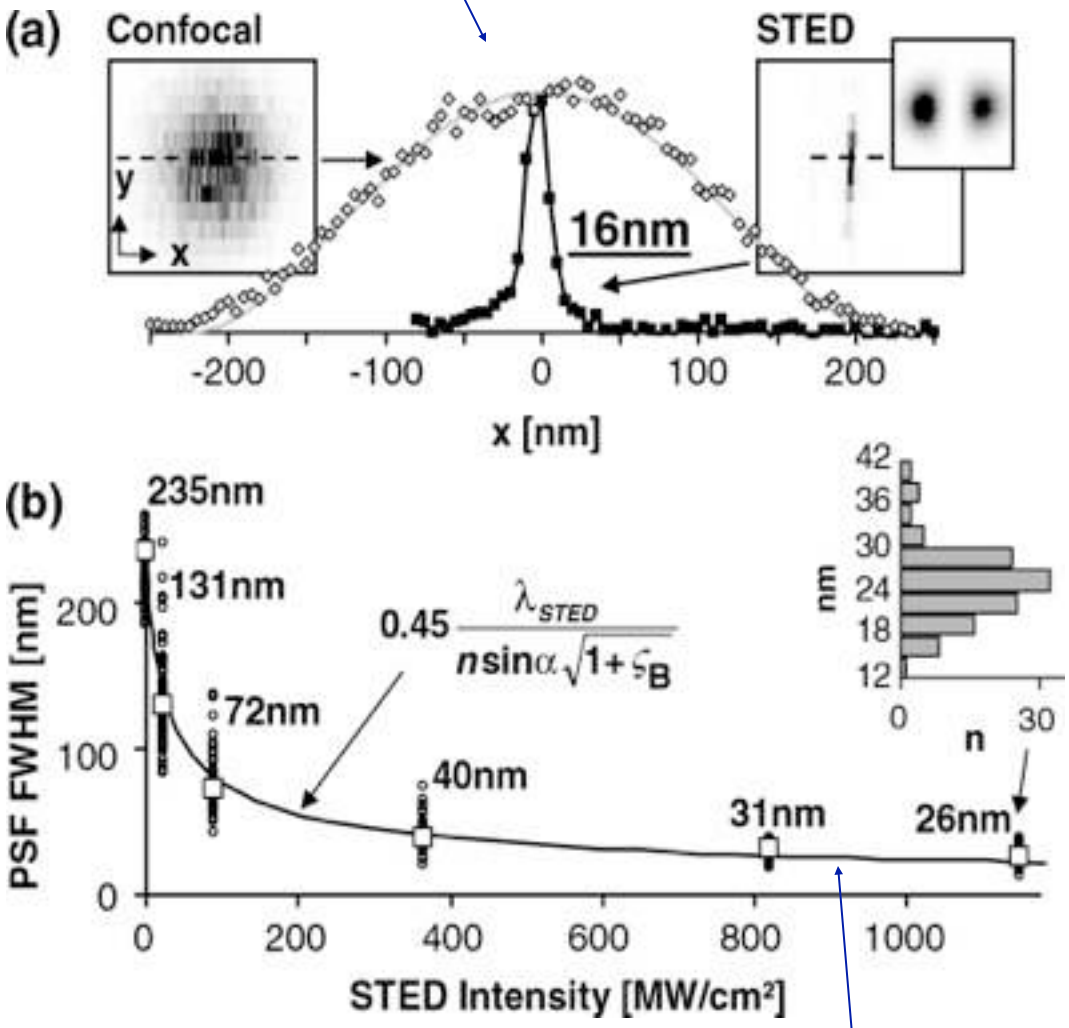

Validation of square-root resolution law

V. Westphal, S.W. Hell (2005), *Phys. Rev. Lett.* **94**, 143903.

Max Planck Society

The combination: STED-4Pi-Microscopy

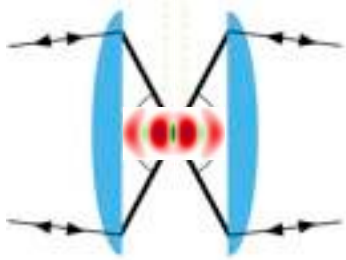

Monolayer

Monolayer

confocal

STED-4Pi

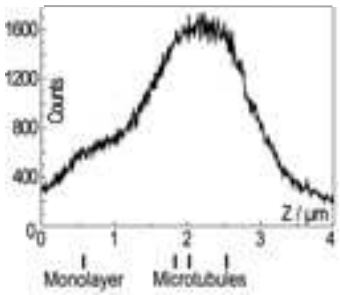

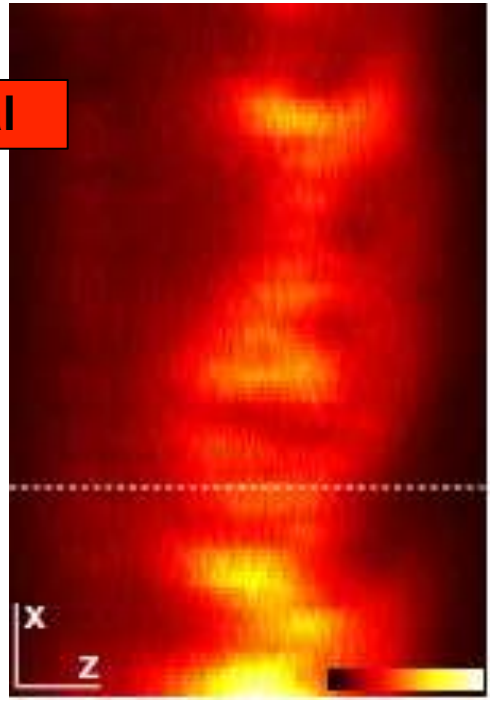

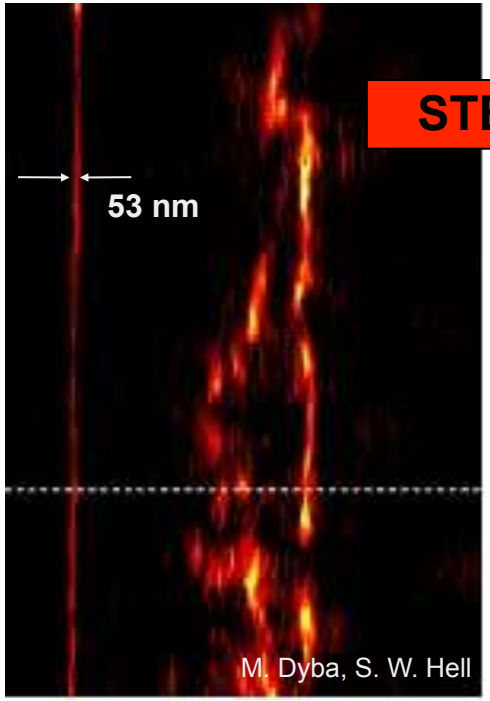

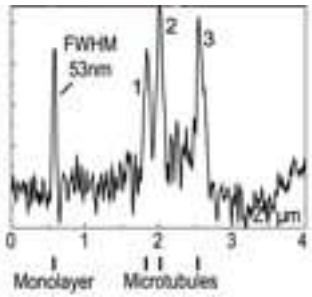

Fluorescently tagged microtubuli
with an axial resolution of 50-70 nm

M. Dyba, S. Jakobs, S.W. Hell (2003), *Nature Biotechnol.* **21**, 1303.

Table 1. Fluorophores for STED microscopy.

Fluorophor	Absorption maximum [nm]	Emission maximum [nm]	STED wavelength [nm]	Additional information	References
Abberior STAR 440 SX	437[a]	515[a]	590–620	–	http://abberior.com
fluorinated rhodamines	512[b] 501[c] 552[d]	530[b] 524[c] 574[d]	590–620 595–615 645–665	rhodamine derivatives, uncaging at 360–440 nm	[78, 165, 166] http://abberior.com
Abberior STAR 635	635[b]	655[b]	740-760	rhodamine derivative	[76, 77] http://abberior.com
Alexa Fluor 594	590	617	700 and 736	–	[54, 167] http://invitrogen.com
Alexa Fluor 488	495	519	592	–	[168] http://invitrogen.com
Atto 425	436	484	532	coumarine like	[169] http://atto-tech.com
Atto 532	532	553	603	rhodamine like	[41, 72, 169] http://atto-tech.com
Atto 565	563	592	650–676	rhodamine like, two-photon excitation	[50, 73, 167, 168, 170] http://atto-tech.com
Atto 590	594	624	700	rhodamine like	[73, 167] http://atto-tech.com
Atto 594	601	627	700	rhodamine like	[167] http://atto-tech.com
Atto 633	629	657	745–750	–	[73, 171] http://atto-tech.com
Atto 647N	644	669	750–780	carborhodamine	[50, 67, 157] http://atto-tech.com
Atto 390	390	479	532	coumarine like	[75] http://atto-tech.com
B504-MA	514	530–540	592	Bodipy like	[60]
Chromeo 488	488	517	592	–	[168] http://activemotif.com
Chromeo 494	494	628	760	long stokes shift dye	[93] http://activemotif.com
Coumarin 102	400	480	532	–	[75]
DY-485XL	485[f]	560[f]	647	–	[59] http://dyomics.com
DY-495	493[f]	521[f]	592	fluorescein-based	[168] http://dyomics.com
DyLight 594	594[f]	615[f]	700	–	[167]
FITC	485	514	592	fluorescein- isothiocyanate	[168]
JA26	635	680	775–781	xanthene like	[70, 172, 173]
KK114	650	670	755	rhodamine like	[74, 76, 167]
MG-2p	632	664	730–750	Malachite green activated by L5-MG-L90S	[95, 96]
MR 121 SE	532	700	793	oxazine like	[39]
Nile red	552[e]	636[e]	765	phenoxazine	[35] http://invitrogen.com
NK51	532	553	647	–	[59] http://atto-tech.com
Oregon Green 488	496	526	592	difluorofluorescein	[168] http://invitrogen.com
PTCA	458	530–540	592	Perylene like	[60]
Pyridine 4	550[f]	770[f]	765	–	[35]
Pyridine 2	500[f]	740[f]	765	–	[35]
RH 414	532[e]	716[e]	765	styryl dye	[35] http://invitrogen.com
TMR-Star	554	580	650	tetramethylrhodamine-derived, permeable	[92] http://neb.com
YOYO-1	491[g]	509[g]	568, 647	dimeric cyanine nucleic acid dye	[105] http://invitrogen.com
GFP	490	510	575	–	[82]
GFP switchable	488	511/515	595	Dronpa-M159T, Padron, on/off at 405 nm	[63]
YFP	514	527	598	–	[84]
Citrine	516	529	592	–	[83, 174]
E2Crimson	611	646	760	tetrameric	[85]
TagRFP657	611	657	750	monomeric	[86]
NV diamond	532	600–850/685	775/740	fluorescent nitrogen vacancy centers	[38, 98]
quantum dots	440 (excitation)	580	676	Mn-doped ZnSe	[97]

[a] in PBS, at pH 7.4, [b] in water, pH 7, [c] at pH7, [d] at pH 7.4, [e] in methanol, [f] in ethanol, [g] dye DNA complexes at pH 7.4. Additional information can be found in the list of dyes used in STED microscopy at http://www.mpibpc.mpg.de/groups/hell

Two color STED

Different Fluorophores can be attached to different proteins:
studies of correlations in positions between proteins
(geometry=function)

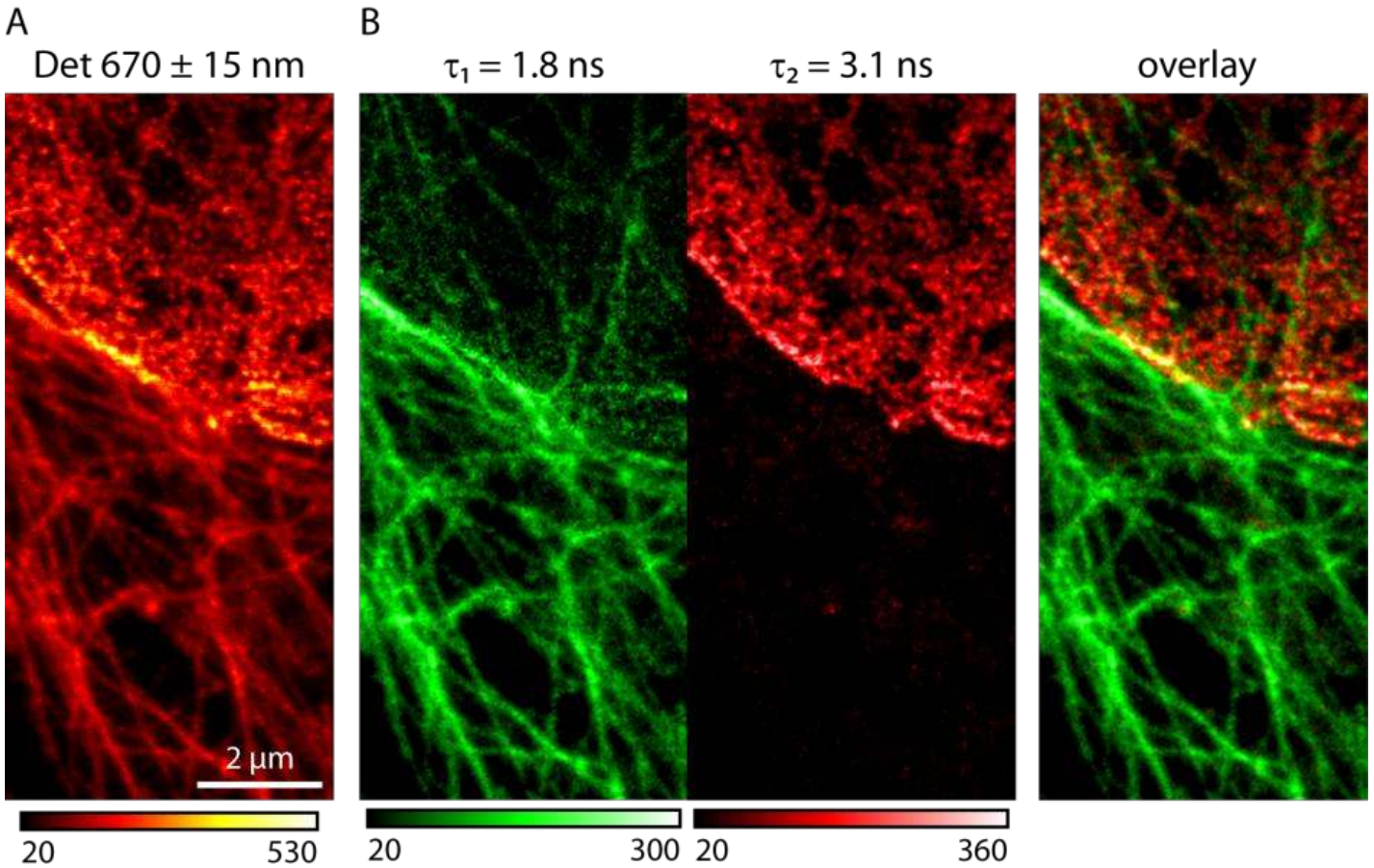

Fig. 3. Two-channel STED imaging by fluorescence lifetime separation. Tubulin and lamin were immunostained with ATTO 647N and KK 114, respectively. (A) Raw intensity STED data and (B) channels decomposed by lifetime separation (green: tubulin, red: lamin).

Cromophores

Photocromism: Reversible photochemical reaction where an absorption band in the visible changes dramatically in strength or wavelength

examples: cyanide dyes, some fluorescent proteins...

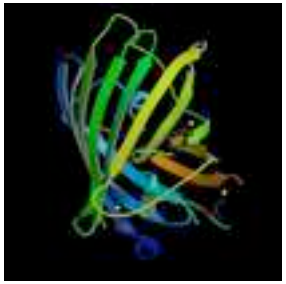

The GFP from A. victoria:

Excitation peak at

λ= 395 nm and 475 nm.

Emission peak at 509 nm

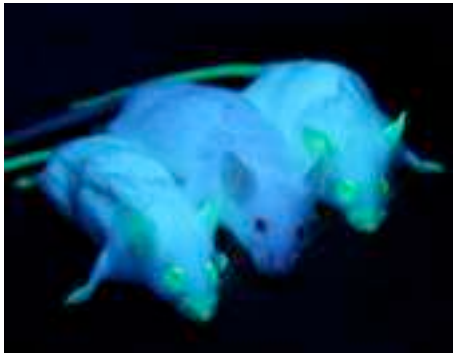

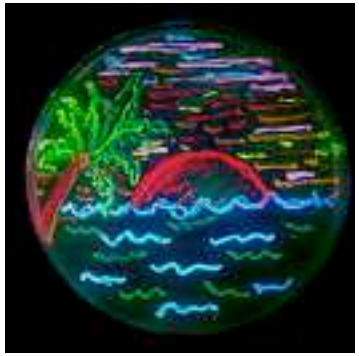

The GFP gene is frequently used as a reporter of expression.

In modified forms it has been used to make biosensors, and many animals have been created that express GFP as a proof-of-concept that a gene can be expressed throughout a given organism.

The GFP gene can be introduced into organisms and maintained in their genome through breeding, injection with a viral vector, or cell transformation.

It is a small fusion protein!

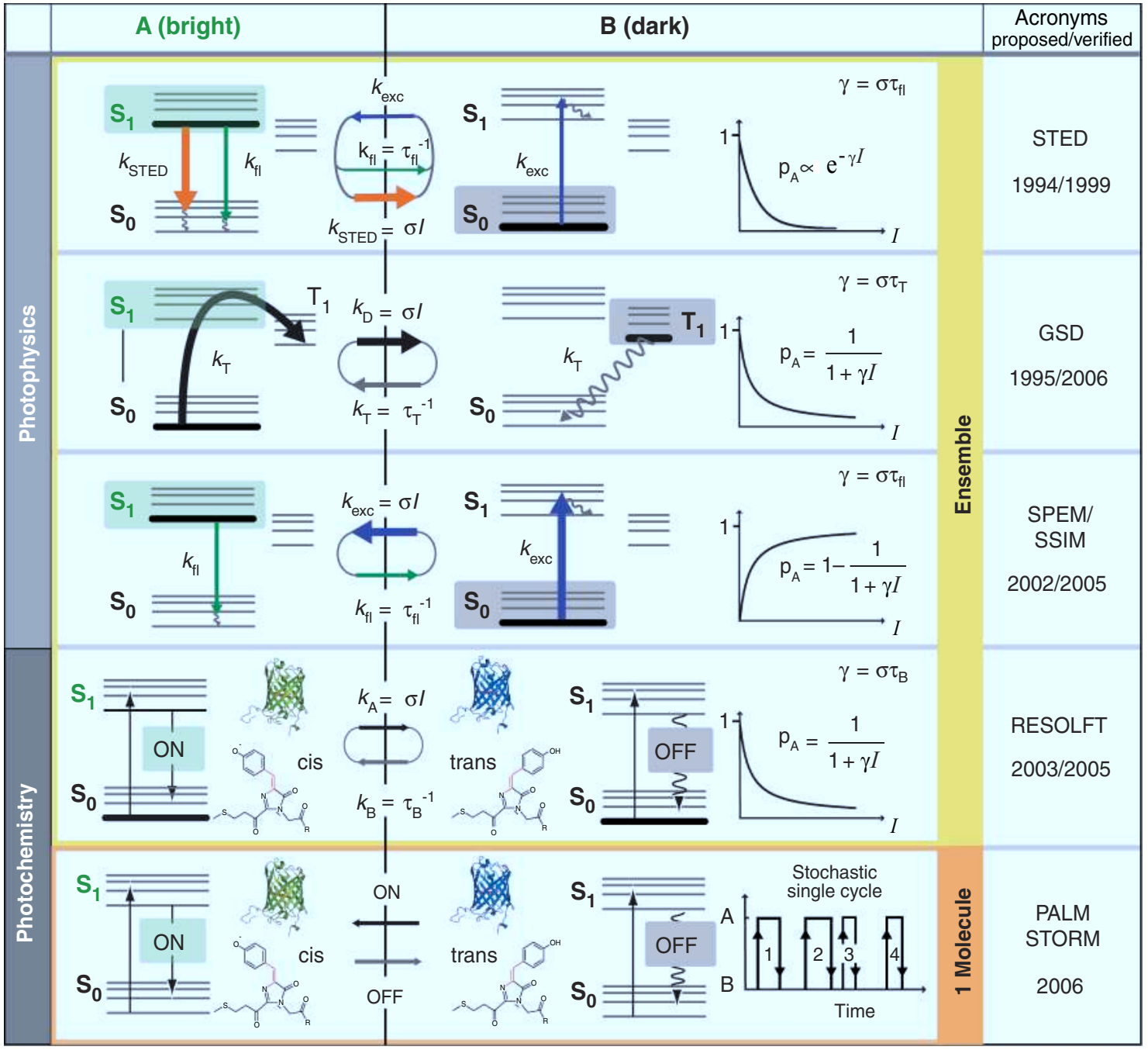

τ=1 ns

I_{sat} =1 MW/cm^2

$$\Delta x \approx \frac{\lambda}{2n\sin\alpha\sqrt{1+I/I_{sat}}}$$

τ=1 ms

I_{sat} =1 W/cm^2

PALM and STORM

Stochastic optical reconstruction microscopy (STORM)
and
Photoativated localization microscopy (PALM)

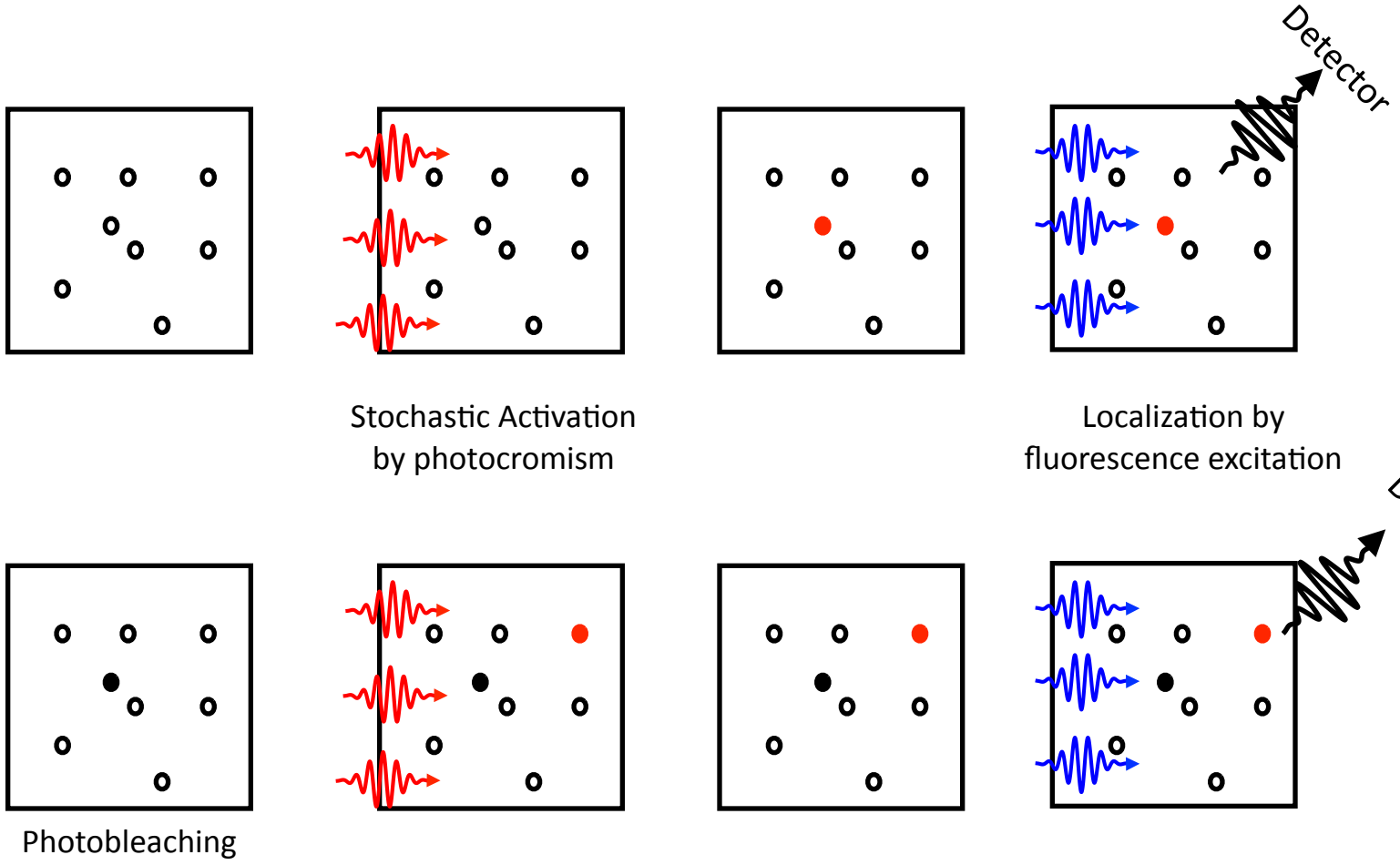

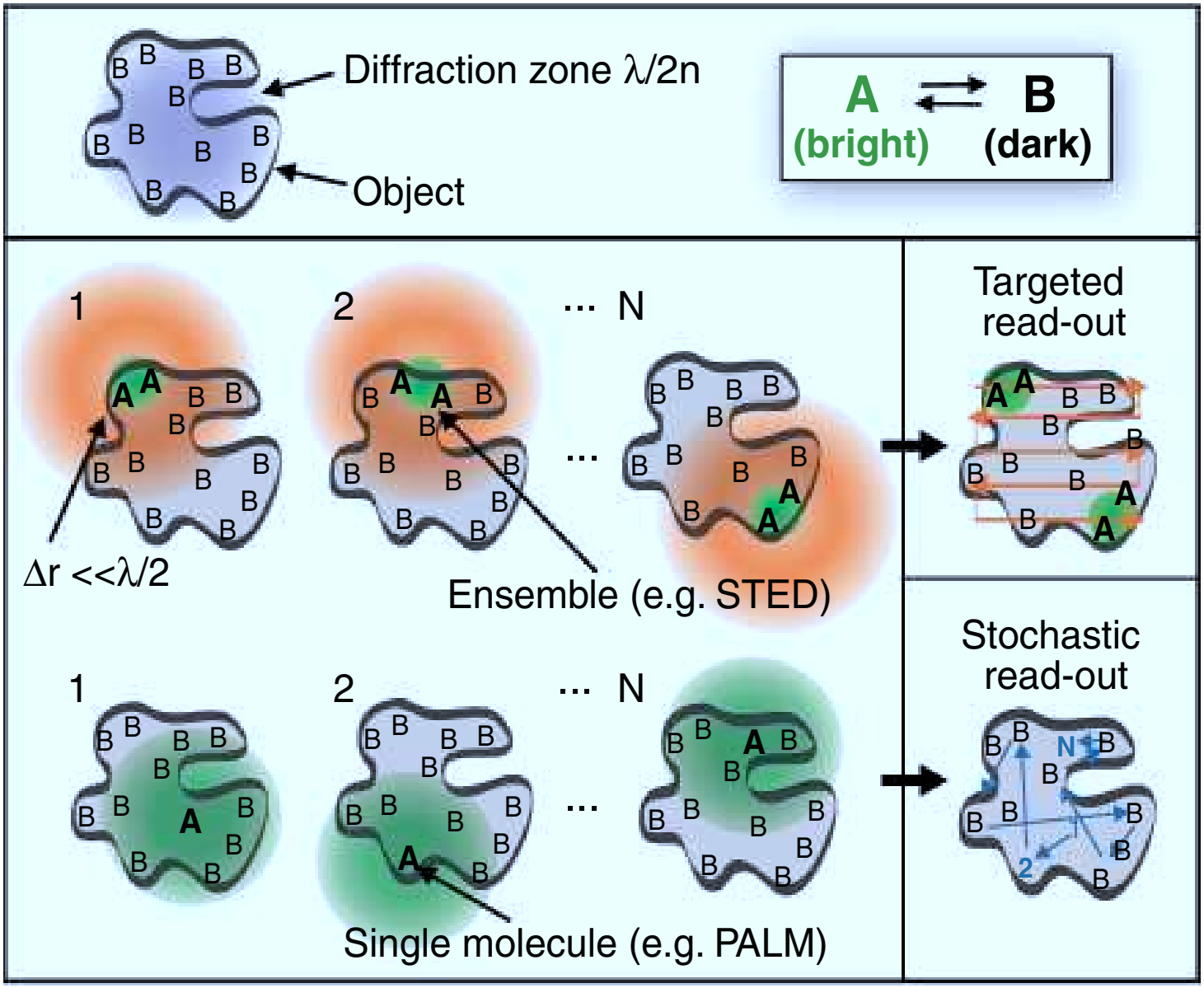
Diffraction zone λ/2n
Object
A (bright) ⇌ B (dark)
1
2
… N
Δr <<λ/2
Ensemble (e.g. STED)
Targeted read-out
1
2
… N
Single molecule (e.g. PALM)
Stochastic read-out

LIMON

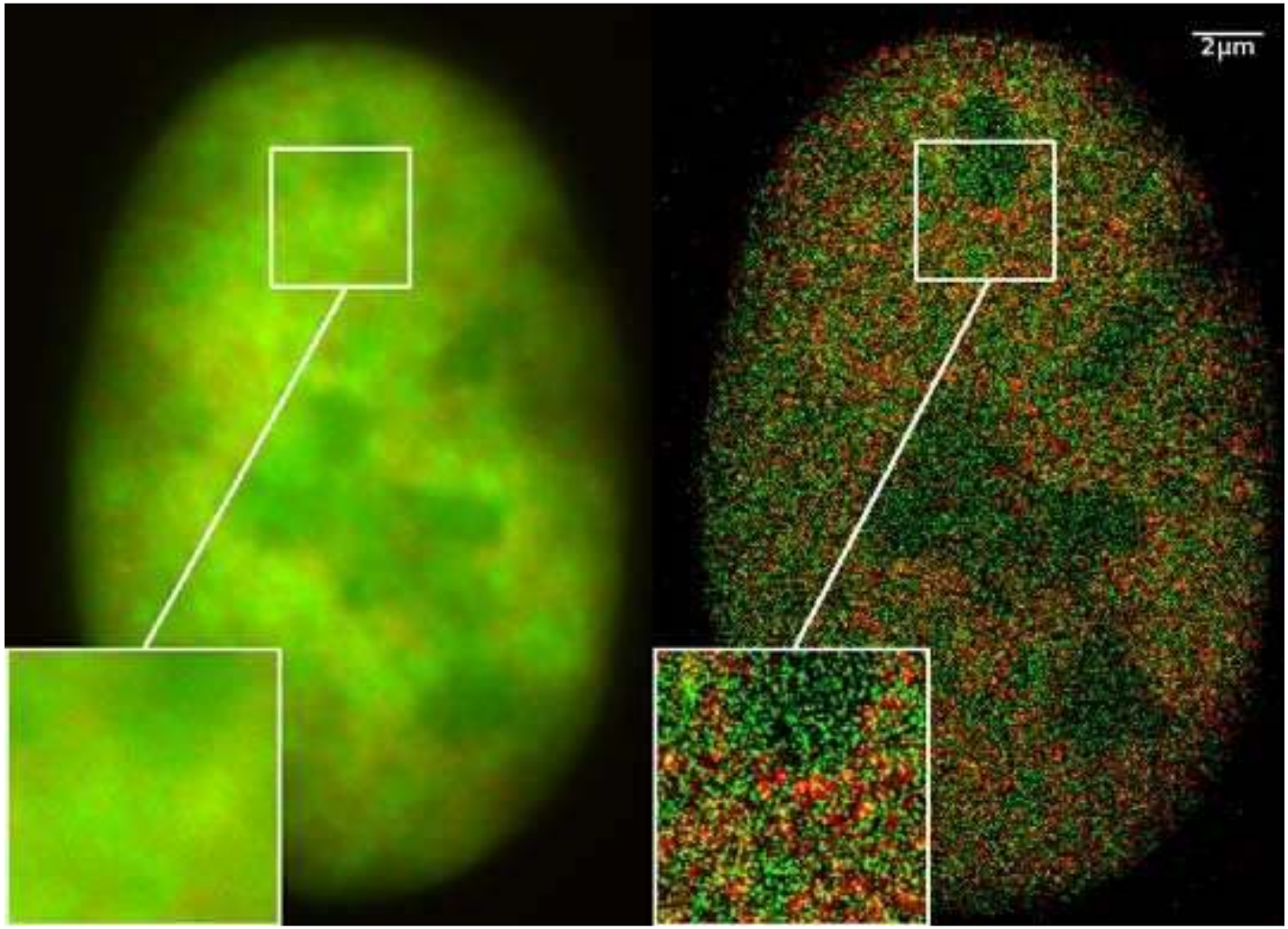

Image/example: View of a nucleus of a bone cancer cell: using normal fluorescence microscopy, it is not possible to distinguish details of its structure (*left*). Using 2CLM /**SPDMphymod** (*right*) it is possible to localize 70,000 histone molecules (red: RFP-H2A) and 50,000 chromatin remodeling proteins (green: GPF-Snf2H) - in a field of view of 470 μm^2 with an optical depth of 600 nm (each spot represents a single molecule, total $1{,}2x10^5$).

Counting individual molecules up to a density of 2,8 • 10^4/µm², this is possible in an area of up to 5000 μm^2 (can be extended to more ca. 125 000 μm^2).

Inmunofluorescence and fusion proteins.

Fusion proteins: DNA included in the DNA of other proteins, so that the cell generates a combination of both.

Different proteins can be targeted with different flourescent fusion proteins, for studies of colocation (and thus correlation of functionalities).

Summary

- Sub-diffraction optical microscopy opens a new era in science

- The key point is to address sequentially emitters with light:

selecting some measurable property and being able to place the rest of emitters in states that do not present that property.

- Only a very small number of possibilities have been explored!